LBL-26709 c.2
Preprint

Lawrence Berkeley Laboratory
UNIVERSITY OF CALIFORNIA

Materials & Chemical Sciences Division

Submitted to Journal of Chemical Physics

UV Photodissociation and Thermochemistry of CH_2BrCH_2I, CF_2BrCF_2I, and CF_2ICF_2I

G.M. Nathanson, T.K. Minton, S.F. Shane, and Y.T. Lee

Janaury 1989

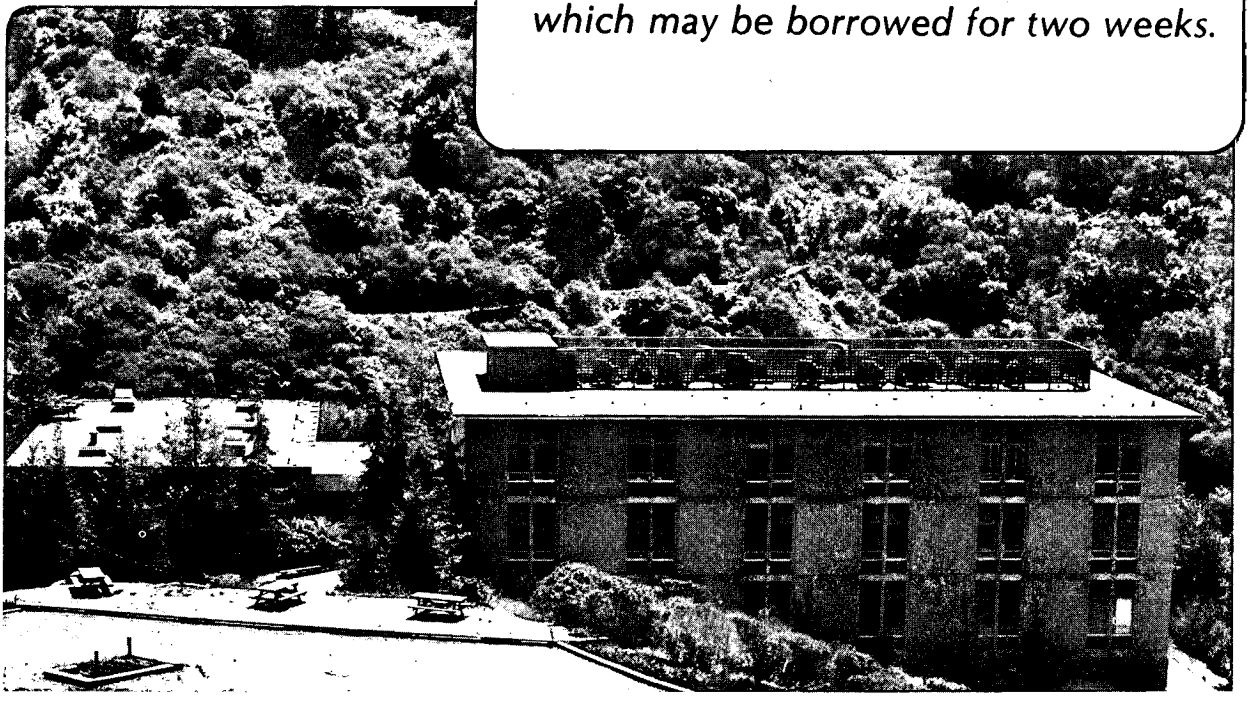

Prepared for the U.S. Department of Energy under Contract Number DE-AC03-76SF00098.

DISCLAIMER

UV photodissociation and thermochemistry of CH_2BrCH_2I, CF_2BrCF_2I, and CF_2ICF_2I

Gilbert M. Nathanson,[a] Timothy K. Minton,[b] Stacey F. Shane[c] and Yuan T. Lee

Materials and Chemical Sciences Division, Lawrence Berkeley Laboratory and Department of Chemistry, University of California, Berkeley, CA 94720

[a] Miller Research Fellow 1985-87. Present address: Department of Chemistry, University of Wisconsin, Madison, WI 53706.

[b] Present address: Physikalisch-Chemisches Institut der Universität CH-8057 Zürich, Switzerland.

[c] Present address: Department of Chemistry, Stanford University, Stanford, CA 94305.

ABSTRACT

Using photofragment translational spectroscopy, we have monitored the dissociation of CH_2BrCH_2I at 248, 266, and 308 nm, and CF_2BrCF_2I and CF_2ICF_2I at 308 nm. The primary fragments are $I(^2P_{3/2})$ and $I(^2P_{1/2})$ and the corresponding haloethyl radicals. The $I(^2P_{3/2})$ contribution decreases upon fluorination, but it is dominant for CH_2BrCH_2I at 308 nm. The electronic absorption dipole lies roughly along the C-I bond axis in every case. Stable CF_2CF_2Br and CF_2CF_2I radicals can be readily generated through photodissociation of the parent compounds, while stable CH_2CH_2Br could not be unambiguously observed. Upper limits to the reaction enthalpy at 0 K for $CF_2ICF_2Br(I) \rightarrow C_2F_4 + I + Br(I)$ are 75 ± 1(59 ± 1) kcal/mol. The TOF spectra and related data suggest that there is a barrier to decomposition for $CF_2CF_2I \rightarrow C_2F_4 + I$ that exceeds the C-I bond energy in the radical.

PACS: 82.50.F, 35.20.G, 82.60.C, 33.80.G

Suggested running title: Photodissociation of Iodohaloethanes

I. INTRODUCTION

Through measurements of the velocities of recoiling fragments, photodissociation experiments reveal how energy is partitioned at the moment of decomposition. This partitioning depends on angular momentum constraints and the extent of energy transfer prior to bond fission, as well as the nature of the interaction potential between the dissociating fragments. Comparative studies of similar molecules show how the shapes of the translational energy distributions mirror small changes in molecular structure and composition. In addition, experiments which can measure limiting velocities imposed by energy conservation afford new opportunities to measure upper and lower bounds for diverse thermochemical quantities in a collision free environment. We have recently pursued these ideas by monitoring the ultraviolet dissociation of the iodohaloethanes and the formation and decay of the internally excited haloethyl radicals produced by C-I bond fission. The results show that electronic excitation of the iodine atom and the stability of the radical depend sensitively on the skeletal atoms. By appropriately choosing these atoms and the laser wavelength, we can generate weakly bound haloethyl radicals with internal energies below their dissociation threshold.

In this paper, we describe results for the ultraviolet decomposition of the iodohaloethanes CF_2ICF_2I and CF_2BrCF_2I at 308 nm, and CH_2BrCH_2I at 248, 266, and 308 nm. These measurements follow previous

studies of CH_2ClCH_2I[1] and CF_2BrCH_2I[2] at all three wavelengths and CF_2BrCF_2I[3] at 248 and 266 nm. This survey of the iodohaloethanes helps to establish a clearer picture of their decomposition and the subsequent chemistry of the free radical products.

Photodissociation Channels

Following absorption of an ultraviolet photon, the iodohaloethane $Y\text{-}CX_2CZ_2\text{-}I$ decomposes along three pathways for X and Z = F or H, and Y = Cl, Br, or I:

<u>C-I bond fission</u>

$$Y\text{-}CX_2CZ_2\text{-}I + h\nu \rightarrow Y\text{-}C\dot{X}_2CZ_2 + I$$

with formation of stable radical

$Y\text{-}CX_2CZ_2$,

possibly followed by spontaneous decomposition

$$Y\text{-}CX_2CZ_2 \rightarrow Y + CX_2{=}CZ_2$$

or photodecomposition

$$Y\text{-}CX_2CZ_2 + h\nu \rightarrow Y + CX_2{=}CZ_2 ,$$

possibly followed by double bond fission

$$CX_2{=}CZ_2 \rightarrow CX_2 + CZ_2$$

<u>C-Y bond fission</u>

$$Y\text{-}CX_2CZ_2\text{-}I + h\nu \rightarrow CX_2CZ_2\text{-}I + Y$$

with formation of stable radical

$CX_2CZ_2\text{-}I$,

possibly followed by spontaneous decomposition

$CX_2CZ_2\text{-}I \rightarrow I + CX_2{=}CZ_2$

or photodecomposition

$CX_2CZ_2\text{-}I + h\nu \rightarrow I + CX_2{=}CZ_2$

<u>three body decomposition</u>

$Y\text{-}CX_2CZ_2\text{-}I + h\nu \rightarrow Y + CX_2{=}CZ_2 + I$

C-I bond fission is the dominant primary process following photon absorption at 248, 266, and 308 nm. Iodine atoms are ejected in the ground electronic state $I(^2P_{3/2})$ (denoted as I) and the spin-orbit excited state $I(^2P_{1/2})$ (denoted as I^*), 21.7 kcal/mol higher in energy. The energy available for translation and internal excitation of the radical is the photon energy $h\nu$ minus the C-I bond energy $D_0^o(C\text{-}I)$ and spin-orbit term E_{so} for the I^* channel. In the experiments performed here, the translational component is measured by the time-of-flight (TOF) technique, and the internal energies are obtained by energy balance. We have observed a rough trend among the five iodohaloethanes for both iodine channels to partition approximately half of the excess energy into translation and half into vibration and rotation of the radical. The distribution is broad enough to prepare the $Y\text{-}CX_2CZ_2$ radicals with a wide range of internal energies. When they are born with an energy exceeding the mechanical barrier for C-Y bond rupture the radicals will spontaneously decompose into Y and the substituted ethylene $CX_2{=}CZ_2$. The free Y atoms are expected to be produced in their ground electronic state, but many radicals contain sufficient energy to decompose into the ethylenic compound and an

excited atom.

The C-Y bonds in the radicals are 40 to 60 kcal/mol weaker than in the parent haloalkanes, since decomposition follows a concerted path that breaks the C-Y bond while forming a new C=C π bond. The π bond in $CF_2=CF_2$ is weaker than in $CH_2=CH_2$ in part because of the unusual stability of singlet CF_2; fluorination effectively strengthens the C-Y bond in the radical by weakening the π bond that forms.[4] Secondary, spontaneous decomposition into Y + $CX_2=CZ_2$ is observed for every molecule in the $I(^2P_{3/2})$ channel, but it occurs less often when $I(^2P_{1/2})$ is ejected since the energy available for breaking the C-Y bond is 21.7 kcal/mol lower. Thus, competition between the I and I^* channels intimately determines the stability of the nascent radical. Since skeletal fluorination increases the I^*/I branching ratio in addition to strengthening the C-Y bond in the radical, stable fluorinated radicals are produced far more abundantly by ultraviolet photodissociation.

Photon absorption and decomposition of the radical can also occur during the same laser pulse that dissociates the parent molecule and creates the radical. We have previously observed photodissociation of CF_2BrCH_2 at 248 and 266 nm, where Br and $CF_2=CH_2$ recoil with velocities larger than allowed by the initial photon absorption.[2] Primary C-Br photodissociation was also postulated at these wavelengths, indicating that the iodine atom may strongly perturb the C-Br absorption spectrum. In earlier studies, Krajnovich et al. recorded spectra of CF_2BrCF_2I which suggest that the CF_2CF_2Br radical photodissociates at 248 nm.[3] The CF_2CF_2-I radical readily absorbs a

second photon at 308 nm; the internal energy is then often sufficient to break both the C-I radical bond and the $CF_2=CF_2$ double bond.

When the excess energy appears predominantly in relative motion of iodine and $Y-CX_2CZ_2$, the radical is internally cold and does not decompose. By measuring the **minimum** internal energy required to break apart the radical, we can estimate an upper limit to the reaction enthalpy ΔH_R at 0 K for the full decomposition $Y-CX_2CZ_2-I \rightarrow Y + CX_2=CZ_2 + I$. ΔH_R equals the sum of the C-I and C-Y bond strengths, and determines the heat of formation of the parent compound from known values of the products. These measurements depend on the appearance of stable haloethyl radicals, which were observed for every species but CH_2CH_2Br. This elusive species is indeed bound, but too little energy is removed in the relative motion of I and CH_2CH_2Br to keep the C-Br bond from breaking. We can estimate the bond energy at 0 K by assuming that $D_0^o(H-CH_2CH_2Br) = D_0^o(H-CH_2CH_3)$ and calculate that $D_0^o(CH_2CH_2-Br) = 6 \pm 1.5$ kcal/mol.[1a] Benson and O'Neal, however, have estimated that this bond energy is near 8 kcal/mol with an activation energy for the reverse addition of less than 3 kcal/mol, so that a total of 11 kcal/mole could be required to break the C-Br bond.[5]

Finally, in some cases photodissociation may not follow the sequential processes described above, but instead proceed directly through three body decomposition. Our results suggest that some CH_2BrCH_2I undergoes nearly simultaneous I and Br elimination at 248 nm, arising perhaps from the strongly overlapping C-Br and C-I absorption bands shown in Fig. 1, and from the relatively low energy required to break the C-I and C-Br bonds. Recently, Taatjes and Leone measured

the Br^*/Br ratio to be >0.1 for CH_2BrCH_2I at 248 nm;[6] the appearance of Br^* further implicates C-Br photon initiated dissociation assuming that only ground state bromine is produced during spontaneous radical decay. We emphasize, however, that it is difficult to discriminate between impulsive C-Br bond fission following direct photon absorption and very rapid secondary dissociation following C-I bond fission.

Within the local, diatomic model of C-I bond photodissociation, ultraviolet absorption excites an iodine nonbonding 5P electron into the lowest unoccupied, antibonding σ^* orbital.[7] $^2P_{3/2}$ and $^2P_{1/2}$ iodine atoms presumably arise from excitation of absorption dipoles which are perpendicular and parallel, respectively, to the C-I bond axis. However, experiments have shown that the transition moment leading to photodissociation in the iodoethanes is always nearly parallel to the C-I axis for **both** iodine states with 248, 266, and 308 nm excitation.[1,2,3,8,9] The production of ground state iodine is attributed to mixing of the strongly repulsive σ^* states in these polyatomic molecules through spin-orbit coupling in the heavy iodine atom.[3,8,9,10] The fully allowed I^* channel is strongest at 266 nm near the C-I absorption maximum shown in Fig. 1, but becomes quite weak at 308 nm for the hydrogen substituted species CH_2BrCH_2I, CH_2ClCH_2I, and CF_2BrCH_2I.

The experiments described below confirm the general conclusions cited above: (1) excess energy is partitioned roughly equally between translation and internal degrees of freedom, (2) the absorption dipole remains nearly parallel to the C-I bond axis at all three wavelengths, despite the prevalence of ground state iodine at 308 nm, and (3) the C-Y bonds in the $Y-CX_2CZ_2$ radicals are very weak

but strengthen upon fluorination, reflecting the isolated C-Y and CX_2=CZ_2 bond strengths.

II. EXPERIMENT

The rotating source photofragment apparatus and experimental technique were described in detail in an earlier paper.[2] The particular conditions for producing beams of each molecule are collected in Table I. A molecular beam is formed by bubbling argon or nitrogen through the liquid reagent and expanding the mixture through a 0.125 mm dia. heated nozzle with a total pressure of 300 torr. The beam is then confined by two skimmers to an angular divergence of 3° and travels 7.4 cm before intersecting a polarized excimer laser at 248 and 308 nm or an Nd:YAG laser at 266 nm. Table I also lists the laser pulse energies and spot sizes. Photofragments at a selected laboratory angle Θ_{LAB} travel 36.8 ± 0.25 cm to the ionizer of the mass spectrometer, where their time of arrival is recorded in one microsecond intervals with a multichannel scaler.

Data is accumulated repetitively at several Θ_{LAB} to obtain angular distributions of the recoiling products. A second method is also used at 248 and 308 nm, where the signal is recorded at a fixed laboratory angle with laser polarizations parallel and perpendicular to the detector axis.

The fluorinated compounds were purchased from SCM Specialty Chemicals, and bromoiodoethane was purchased from Fairfield Chemical Company. CH_2BrCH_2I was determined by GC-MS analysis to contain 5% CH_2ICH_2I; the diiodoethane melts at 83°C, about 43°C above the bath

temperature. The nozzle was heated only to 150°C for this molecule, since decomposition occurred at higher temperatures. For CF_2ICF_2I, molecular beams were formed using both argon and nitrogen as carrier gases at nozzle temperatures of 50°C and 250°C. N_2 suppresses dimer formation better than Ar, but the attendant vibrational and rotational cooling during the expansion is correspondingly worse.

Time-of-flight spectra N(t) were recorded at m/e = 127 (I^+), m/e=79 (Br^+), m/e = 100 ($C_2F_4^+$), m/e = 50(CF_2^+), and m/e = 26 ($C_2H_2^+$). The spectrometer resolution was set low enough to collect a large fraction of the ^{81}Br isotope, and tuned to m/e = 26 to monitor the dissociative ionization of ethylene to avoid the large background at mass 28. We obtained a sufficient signal to noise ratio at m/e = 26 only at 266 nm. Most stable radicals dissociatively ionize upon electron impact and could not be detected directly, with the exception of CF_2CF_2I at 308 nm. Table I indicates representative time-integrated signal levels in ion counts/laser pulse for the three molecules. The flight time in microseconds from the ionizer to the detector is $\alpha(\text{amu})^{1/2}$. α = 4.0 $\mu s/(\text{amu})^{1/2}$ for experiments using Ar carrier gas and 4.2 $\mu s/(\text{amu})^{1/2}$ for experiments using N_2.

III. RESULTS AND ANALYSIS

A. Methods of Analysis

The laboratory TOF spectra are the raw data used to compute the center-of-mass(c.m.) energy distributions, anisotropies (distribution of recoil directions with respect to laser polarization), and I^*/I branching ratios. The probability $p(\theta_{cm}, v_{cm})$ of the angular and

velocity distributions of the fragments in c.m. coordinates is recovered from the laboratory data using the prescription $p(\theta_{cm},v_{cm}) = v^2_{cm}/V^2_{LAB}\ p(\theta_{LAB},V_{LAB})$, convoluted over the distribution of parent beam velocities and the effective length of the ionizer. We assume that $p(\theta_{cm},E_{cm})$ is equal to a product of functions $T(\theta_{cm})P(E_T)$, where $T(\theta_{cm}) = 1 + \beta P_2(\cos\theta_{cm})$ for electric dipole absorption.[11] θ_{cm} is the angle between the laser polarization and detector axes. For a direct dissociation from a repulsive state, β reflects the orientation of the transition moment with respect to the bond dissociation axis; β is 2 when the dipole is parallel to the dissociation coordinate and -1 when perpendicular. Rotation and distortion of the excited complex drive β toward smaller (absolute) values. When only two body dissociation occurs, momentum conservation determines the recoil energy of the unobserved fragment, and the c.m. distribution of total translational energies $P(E_T)$ can be calculated. For three body dissociation, limited information can be obtained when all three fragments are observed.[12]

Sequential, two body dissociation is more difficult to analyze. Kroger and Riley first formulated an elegant solution in their studies of acetyl iodide photodissociation.[13] We use an alternative procedure that will be described in a separate report.[14] For the secondary dissociation of CF_2CF_2I into $CF_2{=}CF_2$ and I at 308 nm, we have made an estimate of the average recoil energy of the products by modeling the $CF_2CF_2^+$ TOF spectrum. This data, shown later in Fig. 8, displays a characteristic bump at flight times shorter than the stable radical signal and indicates that the secondary products are recoiling from each other at substantial velocities.

B. CF_2BrCF_2I at 308 nm

Representative I^+ TOF spectra are shown in Fig. 2 at θ_{LAB} = 20°, 40°, and 50°. In analogy with previous studies, the fast and slow peaks are assigned to iodine atom recoil in the primary dissociation $CF_2BrCF_2I \rightarrow CF_2CF_2Br + I(I^*)$. By energy conservation, the fast peak must be ground state iodine(I) while the slower peak is assigned to excited state iodine(I^*). The dashed lines indicate a likely deconvolution, and the solid line is the overall fit to the data. The total c.m. translational energy distribution $P(E_T)$ is displayed in the bottom panel, illustrating I and I^* contributions of 23% and 77%. The arrows mark the energy available for translation, E_{avl}, determined by $h\nu - D_0^\circ(C\text{-}I)$ = 92.8 - 52 = 40.8 kcal/mol for the $I(^2P_{3/2})$ channel and 40.8 - 21.7 = 19.1 kcal/mol for the $I(^2P_{1/2})$ channel. The internal energy initially in the parent molecule is excluded from this estimate, but a fraction of it can also be channeled into translation. $D_0^\circ(C\text{-}I)$ is assumed to equal the bond energy for $CF_3CF_2\text{-}I$, since the C-I bond strengths are not precisely known for the iodohaloethanes. The average translational energy release $\langle E_T\rangle/E_{avl}$ for each channel is .60 for I and .73 for I^*. Separate fits to the time integrated signal at 20° through 50°, and at 40° with parallel and perpendicular laser polarizations, determine the anisotropy to be $1.2<\beta<1.8$ for both iodine states.

The TOF spectrum of $CF_2CF_2^+$(m/e = 100) is shown in the top panel of Fig. 3; $CF_2CF_2^+$ is generated by dissociative ionization of the stable radical CF_2CF_2Br and direct ionization of $CF_2{=}CF_2$. The two peaks

are produced by recoil of stable radical through the I and I^* channels of the primary dissociation. The slow peak is fit well by using the $P(E_T)$ derived from the excited state iodine TOF spectrum, indicating that all CF_2CF_2Br radicals from the I^* channel remain stable. The fast peak lacks slow signal predicted from the ground state I channel, shown by the dotted line, implying that the slower, more internally excited CF_2CF_2Br decomposes into CF_2CF_2 and Br. The recoiling CF_2CF_2 appears at longer and shorter flight times, adding to and distorting signal from both channels.

An upper limit to the reaction enthalpy is determined by measuring the slowest arrival time for stable CF_2CF_2Br; this flight time determines the minimum translational energy release E_{min} and by energy balance the maximum internal energy for surviving radicals.[1] The energy required to break both C-I and C-Br bonds, $\Delta H_R(0)$, is less than or equal to $h\nu - E_{min}$ ($-E_{so}$) for $I(I^*)$ by energy balance. Our results determine an upper bound to ΔH_R since there may be a mechanical barrier to dissociation in excess of the bond energy. Trial fits to the trailing edge of the peak in Fig. 3 correspond to total c.m. translational energies $E_{min} = 19 \pm 2$ kcal/mol, shown in the bottom panel. The enthalpy for the reaction

$$CF_2BrCF_2I \rightarrow CF_2CF_2 + I + Br$$

at 0 K is then $h\nu - E_{min} = 92.8 - 19 = 73.8 \pm 2$ kcal/mol. Approximately 65% of the radicals produced in the ground state iodine channel are stable, so that 90% of all nascent CF_2CF_2Br remain intact at 308 nm. The same value of E_{min} was measured by substituting N_2 seed gas at a nozzle temperature of 50°C for argon at 250°C. Possible sy-

stematic errors in determining the reaction enthalpy will be discussed later.

Since the trailing edge of the fast peak in Fig. 3 is partly obscured, we repeated the experiment at 266 nm, and obtained the $CF_2CF_2^+$ spectrum shown in the upper panel of Fig. 4. The nearly flat secondary dissociation signal has been subtracted from the data, so that signal from the stable radical disappears at the baseline. Only excited state iodine is produced at this wavelength, and the slowest arrival times for the stable radical correspond to E_{min} = 11 ± 1 kcal/mol. The reaction enthalpy for this measurement is $h\nu - E_{so} - E_{min}$ = 107.5 - 21.7 - 11 = 74.8 ± 1 kcal/mol, close to the value above. At 266 nm, 65% of the radicals remain stable.

C. CF_2ICF_2I at 308 nm

Representative TOF spectra at m/e = 127, m/e = 100, and m/e = 50 using an unpolarized excimer laser are shown in Figs. 5 through 8. The parent molecules were seeded in N_2 at a nozzle temperature of 50°C, in order to reduce the parent internal energy and still limit clustering. Several processes contribute to the I^+ spectra: $I(I^*)$ from primary dissociation of CF_2ICF_2I, $I(I^*)$ from spontaneous and stimulated dissociation of the CF_2CF_2I radical, and iodine from dissociative ionization of stable CF_2CF_2I. The dominant peak at θ_{LAB} = 20° in Fig. 5 is I^+ from primary iodine in the I^* channel, while the slower and smaller peak is dissociative ionization of stable radical. The laser power dependence of the iodine signal indicates that both primary iodine and stimulated dissociation of CF_2CF_2I contribute to the fast

shoulder. Spontaneous dissociation of hot CF_2CF_2I makes up much of the remaining broad signal. The time-integrated iodine signal is apparently linear in laser fluence up to $3x10^{18}$ photons cm^{-2} $pulse^{-1}$.

A rough estimate of the translational energy distribution for the primary dissociation fragments can be obtained by fitting the I^+ signal at wide angles, where I^+ from CF_2CF_2I or from slowly recoiling products of the decomposition of the radical cannot contribute. The fit to θ_{LAB} = 70° is shown in Fig. 5; the fast component is composed of both primary $I(^2P_{3/2})$ and of iodine from stimulated dissociation of the radical, as indicated by its power dependence. The primary $I(^2P_{1/2})$ channel dominates the larger and slower peak and contributes roughly 70% of the signal. The calculated fit for this process is shown in Fig. 5, and yields $\langle E_T \rangle$ = 14 kcal/mol. The shape of the $P(E_T)$ changes very little when the nozzle is heated to 250°C or when the laser power is increased.

The $CF_2CF_2^+$ TOF spectra mirror the processes observed in the I^+ spectra. The most prominent feature is $CF_2CF_2^+$ from dissociative ionization of stable radical, whose trailing edge determines E_{min}. Figs. 6 and 7 show five fits to the stable radical peak under conditions of differing laser power, seed gas, ion mass, and nozzle temperature. In each panel, the estimated trailing edge of the stable radical signal has been set to zero by subtracting the nearly constant secondary dissociation signal. Additional spectra were recorded when $C_2F_4I_2$ was seeded in argon at 50°C, when θ_{LAB} = 15°, and when monitoring the CF_2^+ fragment. All spectra are fit by E_{min} = 12 ± 2 kcal/mol, and most fall within ± 1 kcal/mol. These results yield ΔH_R = 92.8 - 21.7

- E_{min} = 59.1 ± 1 kcal/mol. The calculated solid line fits in each panel were derived from fitting the $CF_2CF_2^+$ spectrum in the top panel of Fig. 6 using the $P(E_T)$ in Fig. 7. The higher temperature spectrum in Fig. 7 differs on the slow side from those in Fig. 6 because of spontaneous dissociation of a substantial fraction of the radicals whose parent molecules acquired extra internal energy at the heated nozzle. The $P(E_T)$ for this spectrum is also shown in Fig. 7, and its more gradual rise reflects the broader distribution of parent internal energies. The similarity between the TOF spectra using argon carrier gas at a nozzle temperature of 250°C and nitrogen at 50°C suggests that the vibrational temperatures are very similar and that argon is much more efficient in relaxing vibrational degrees of freedom. The relative cooling rates are reflected in the substantial clustering observed with argon at 50°C in comparison with nitrogen at the same nozzle temperature.

RRKM estimates and direct time-resolved measurements by Zewail and coworkers[15] point to picosecond lifetimes for vibrationally excited CF_2CF_2I radicals, so that at low laser fluence only radicals that are stable or have internal energies just above the dissociation threshold are likely to photodissociate. Photon absorption by the radical appears to depend weakly on its internal energy; the spectra in Fig. 6 show that the stable radical $C_2F_4^+$ spectra at high and low laser fluence have very similar shapes, although the change in internal energy in the radical across the spectrum is 7 kcal/mol. This is in contrast to the temperature dependence of the primary iodine signal, which increases by roughly a factor of five over the nozzle

temperature range of 50°C to 250°C, after correcting for the decrease in beam density at the higher temperature.

The secondary $CF_2CF_2^+$ signal shown in the top panel of Fig. 8 also indicates that dissociation of CF_2CF_2I increases rapidly with nozzle temperature. The sharp central spike is dissociative ionization of stable radical, and the faster peak and underlying background indicate radical dissociation into C_2F_4 and I. The average internal energy in the parent molecule at 250°C before expansion is 10 kcal/mol, while at 50°C it is 4.5 kcal/mol. The average internal energy imparted to the radical fragment by photodissociation is $h\nu - D_0^o(C\text{-}I) - E_{so} - \langle E_T \rangle$ = 92.8 - 52 - 21.7 - 14 = 5 kcal/mol. Thus, the parent internal energy plays a prominent role in determining whether decomposition of CF_2CF_2I can occur with a dissociation energy nominally equal to $\Delta H_R - D_0^o(C\text{-}I)$ = 59 - 52 = 7 kcal/mol. Approximately half of the radicals created in the primary dissociation remain stable at fluences of 4×10^{17} photons cm^{-2} $pulse^{-1}$ at a nozzle temperature of 50°C.

Spectra in the second and third panels of Fig. 8 show the laser fluence dependence at 3 and 40×10^{17} photons cm^{-2} $pulse^{-1}$ for $C_2F_4^+$ and CF_2^+ at 50°C. These spectra suggest that the fast peak at low and high laser power adjacent to the stable radical signal is spontaneous secondary dissociation into C_2F_4 and I, while the fastest signal is stimulated dissociation of the radical. Secondary photodissociation actually causes the stable radical signal to decrease at high laser fluences. The $CF_2{=}CF_2$ attributed to spontaneous dissociation of the radical recoils at low velocities, and the signal rises less rapidly with laser power than the linearly increasing primary signal. Thus,

some radicals that would have decomposed spontaneously may instead be photodissociating at high laser fluence.

Approximate fits to the spontaneous secondary dissociation signal using an RRK form[16] for the $P(E_T)$ indicate average total c.m. translational energies for $CF_2CF_2I \rightarrow C_2F_4 + I$ of 3 to 5 kcal/mole. If the C_2F_4 observed at this low recoil energy were to be created by photodissociation of the radical, then its internal energy would exceed the double bond strength of $CF_2=CF_2$ by more than 15 kcal/mol. Thus, the appearance of C_2F_4 at low c.m. translational energies is consistent with a spontaneous dissociation pathway for CF_2CF_2I.

The bottom panel in Fig. 8 compares spectra monitored at CF_2^+ and $C_2F_4^+$ at 50°C and high laser power. The CF_2^+ spectrum reveals at least one extra peak at fast times, attributable to photon absorption of the radical, followed by C-I and double bond fission of the radical into $CF_2 + CF_2 + I(I^*)$. This new peak is also evident in the high power CF_2^+ spectra in the third panel. The highest velocity CF_2 fragments are consistent with estimates of the strength of the double bond in $CF_2=CF_2$,[17] but the uncertainty in the flight time of the rising edge prohibits an independent measurement of the double bond strength.

D. CH_2BrCH_2I at 248, 266, and 308 nm

1. I^+ TOF Spectra

Representative m/e = 127 TOF spectra recorded at three wavelengths are shown in Figs. 9, 10, and 11. Assuming two body dissociation of CH_2ICH_2Br into I and CH_2CH_2Br, we have fit these spectra using the energy distributions shown in Fig. 12. The available

energies are calculated using the C-I bond energy at 0 K of 54.5 kcal/mol for CH_3CH_2-I.[1a]

At 266 nm, the fast component is assigned to the $I(^2P_{3/2})$ channel and the dominant slower peak to production of $I(^2P_{1/2})$. One likely deconvolution is shown in Fig. 12, which yields a branching ratio of $I^*/I = 9:1$. The average translational energy $\langle E_T \rangle / E_{avl}$ for each channel is 0.47 for I^* and .42 for I. In order to derive the $P(E_T)$ which fits the wide angle data accurately, we found that a portion of the slow signal at small angles fell outside the calculated curve. This slow component at $\theta_{LAB} = 20^\circ$ grows quickly as the nozzle temperature is reduced from 150°C to 90°C, indicating that the unfitted signal is produced by dissociative ionization of parent molecules recoiling slowly from photodissociated clusters.

The fast and abrupt shoulder in the 248 nm spectra in Fig. 10 does not have the shape typically associated with the $I(^2P_{3/2})$ channel.[1-3] It extends at fast times to the available one photon energy limit but not beyond, and may extend at slow times underneath the large peak. The $P(E_T)$ which fits the overall data is shown in Fig. 12; the slower, dominant peak is assigned to the $I(^2P_{1/2})$ channel, for which $\langle E_T \rangle / E_{avl} = 0.48$. All dissociation events with energy higher than E^*_{avl} plus the parent internal energy must belong to the ground state channel, but this minimum value is less than 2.5%. The fast shoulder contributes at least 5% of the signal, but its origin is uncertain.

The 308 nm TOF spectra in Fig. 11 reveal a smooth distribution of points, and the derived $P(E_T)$ is a sharply peaked curve, which is assigned to the $I(^2P_{3/2})$ channel by energy conservation. The broadening

of the $P(E_T)$ in Fig. 12 at energies lower than E^*_{avl} suggests that a fraction of the dissociation events may follow the excited state channel, which makes an estimated maximum contribution of 20%. $<E_T>/E_{avl}$ equals 0.43 assuming that the $I(^2P_{3/2})$ channel accounts for the entire distribution. This strong bias toward the ground state channel at 308 nm was also observed for CH_2ClCH_2I, where over 80% of the events lead to $I(^2P_{3/2})$.[1]

The laboratory angular distributions at 20°, 30°, 40°, and 50° for the overall signal determine the anisotropy to be $0.8<\beta<1.8$ at 248 nm, $1.5<\beta<2.0$ at 266 nm, and $0.9<\beta<1.9$ at 308 nm. Further fixed angle, parallel and perpendicular polarization scans at $\theta_{LAB} = 20°$ limit β near 1.9-2.0 at 248 nm and 1.6-1.8 at 308 nm.

2. Br^+ and $C_2H_2^+$ TOF Spectra

The m/e = 79 and m/e = 26 TOF spectra are shown in Figs. 13 and 14.

a. 308 nm. Only one Br^+ spectrum was recorded because of the weak signal at 308 nm. The solid curve is the predicted Br^+ signal from dissociative ionization of CH_2CH_2Br derived from the I^+ $P(E_T)$ assuming that no radicals undergo decomposition. The smooth distribution of data points does not reveal a sharp break separating stable radical from free Br atoms, thus prohibiting a determination of the reaction enthalpy. The maximum literature prediction for ΔH_R is 66 kcal/mol, using a C-I parent bond energy of 55 kcal/mol and a C-Br radical bond

energy of 11 kcal/mol.[5] This value implies that the radical would be stable at flight times faster than 270 microseconds. The I^+ $P(E_T)$, however, shows that fewer than 1% of the radicals are created with such high translational energies. The sharp and fast signal in this spectrum may indicate that the secondary dissociation is extremely rapid, reflecting the anisotropy of the primary bond fission.

b. 248 nm. The Br^+ spectra at θ_{LAB} = 20° and 50° are shown in the bottom two panels in Fig. 13. The solid curves are the predicted flight time profiles for dissociative ionization of CH_2CH_2Br based on the 248 nm I^+ $P(E_T)$. There is again no clear delineation between Br^+ arising from stable radical and from free Br atoms. CH_2CH_2Br radicals are expected to be stable when arriving earlier than 260 microseconds, which occurs near the peak of the spectrum. According to the I^+ $P(E_T)$ for the I^* channel, however, fewer than 5% of the dissociation events impart the primary fragments with such high translational energies, and stable CH_2CH_2Br cannot be unambiguously isolated in this spectrum.

We expect that the bromine signal arises mostly from secondary dissociation of CH_2CH_2Br but we cannot rule out the possibility that direct CH_2ICH_2-Br photodissociation plays a significant role; the absorption spectrum in Fig. 1 indicates that C-Br excitation is likely at 248 nm. A third process which could contribute is photodissociation of the radical, but there is no evidence for fast bromine atoms exceeding the one photon energy limit. The spectra in Fig. 13 at 20° and 50° can be fit well by assuming primary dissociation into Br and CH_2CH_2I with β=1.7 and a $P(E_T)$ that peaks at 16 kcal/mol

with a FWHM of the same value. The CH_2CH_2I radical, however, is not bound and it is likely that nearly instantaneous three body dissociation occurs as the C-Br bond breaks. The I atom ejected during this process may be responsible for the fast shoulder in the I^+ TOF spectra, which is absent in the Br^+ spectra. We note that a similar but weaker I^+ fast component was observed in the 248 nm dissociation of CF_2BrCH_2I, in addition to both the I and I^* channels. In this case, direct C-Br bond fission produces weakly bound CF_2CH_2-I radicals that undergo further dissociation.[2]

c. 266 nm. Br^+ and $C_2H_2^+$ spectra at $\theta_{LAB} = 20^\circ$ are shown in Fig. 14. In these spectra, a fast shoulder is adjacent to a dominant and slowly decaying peak, mirroring the two I and I^* peaks in the iodine spectra. The solid and dashed component curves are predictions for dissociative ionization of CH_2CH_2Br if all radicals remained stable following the primary I and I^* paths. The predicted curves overlap with the sharp peak in the m/e = 79 spectrum, but the overlap is small at m/e = 26. There are no visible momentum matched features in Br^+ and $C_2H_2^+$ spectra originating from dissociative ionization of the radical. Based on the deconvolution of the I^+ $P(E_T)$ in Fig. 10, we do not expect any stable radical to survive in the I channel, and less than 2% to survive in the I^* channel. The two peaks in the Br^+ and $C_2H_2^+$ spectra may largely reflect secondary dissociation of CH_2CH_2Br created by the two I and I^* routes of the primary dissociation.

IV. DISCUSSION

A. Electronic Excitation and Energy Partitioning

The quantitative results from these experiments, along with previous measurements for CF_2BrCH_2I and CF_2BrCF_2I, are collected in Table II.[18] They provide an opportunity to determine how skeletal F and H atoms modify the photochemistry of $Br-CX_2CZ_2-I$. We find that F and H substitutions primarily affect the I^*/I branching ratio and stabilities of the radicals. The thermochemical results are discussed in the next section.

The anisotropies of $\beta>1$ for each molecule indicate that the absorption dipole is aligned roughly along the C-I bond axis at 248, 266, and 308 nm. In cases where the two spin-orbit states of iodine can be resolved, the anisotropies are very close. There is, however, little correlation between β and the I^*/I branching ratio. The ground state iodine channel is strongly inhibited by fluorination but is dominant for CH_2BrCH_2I, CH_2ClCH_2I, and CF_2BrCH_2I at 308 nm. The hydrogen substituted species also have significant $I(^2P_{3/2})$ contributions at 248 nm,[1,2,8,9,19] but for CH_2BrCH_2I this channel appears to be anomalously low; three body dissociation and direct C-Br absorption make the assignment of the fast shoulder to the $^2P_{3/2}$ channel uncertain. The fluorine substituent effect has been noted many times before, and can be correlated with both the increasing ionization potential[9] and mass[20] of the haloalkyl group. Our results at 308 nm show that these effects are strongly wavelength dependent, reflecting the shapes and intersections of the repulsive excited state surfaces. The larger fraction of $I(^2P_{3/2})$ atoms at 308 nm for all species increases the

number of radicals with high internal excitation, and reduces the number that remain stable. Thus, photodissociation at longer wavelengths does not necessarily lead to products with less internal excitation; the internal energies of the CH_2CH_2Br radicals at 248 and 308 nm are quite similar, and in both cases exceed the C-Br bond strength.

The average partitioning of energy between translation and the internal modes of the radical varies weakly with fluorination. The average translational energies cluster within 0.55 ± 0.15, and increase with the mass of the radical mainly at 308 nm. The values of $\langle E_T \rangle / E_{avl}$ are somewhat lower than predicted by the equilibrium geometry rigid radical model (RR), which ignores vibration and determines the rotational excitation from the impulsive torque as the radical and iodine atom separate.[8] The soft radical model (SR), which constrains the initial impulse to occur between the iodine and attached carbon atoms,[21] predicts values that are too low and that shift in the wrong direction with radical mass.

The widths of the translational energy distributions, expressed as FWHM/$\langle E_T \rangle$, do increase with full fluorination of the radical, and the broad distributions for CF_2BrCF_2I have been noted before.[3] The fractional widths for CF_2BrCH_2I and CH_2BrCH_2I are within 0.1 at 248 and 266 nm, despite the increase in the number of vibrational modes below 500 cm^{-1} from 4 to 8 in the difluoro compound. At 308 nm, the FWHM/$\langle E_T \rangle$ values lie between 0.3 to 0.45, with the exception of the broader fractional width of 0.55 observed for CF_2ICF_2I. Iodine electronic excitation also has a modest effect. The $I(^2P_{3/2})$ channels

have larger absolute widths but smaller relative ones, suggesting that the extra 21.7 kcal/mol is channeled with low dispersion and roughly equally into the internal and translational modes. The similarity among the widths and average values of E_T reflects the very short time available for energy redistribution during C-I bond fission, as well as angular momentum constraints imposed by the rigidness of the radical framework. Within the rigid radical model, the nascent Y-CX_2CY_2 will be rotating rapidly, with angular momentum J exceeding 150 $\hbar$ at peak translational energies. This rotational excitation can later appear in the relative motion of the secondary products.

Molecules in the less stable gauche configuration can also alter the measured $P(E_T)$, since they have larger equilibrium impact parameters and should channel less energy into translation. Under conditions in which the populations are locked at a nozzle temperature of 250°C, the gauche conformers will contribute roughly 10% for CH_2BrCH_2I, 20% for CF_2ICF_2I, and 30% for CF_2BrCF_2I.[22] Our temperature studies of CF_2ICF_2I at 50°C and 250°C in N_2, however, do not reveal significant broadening of the I^* $P(E_T)$ fitted to the I^+ spectra at θ_{LAB} = 70°. The gauche conformers may play a more important role in electronic energy transfer, since the C-I and C-Y dipoles will no longer be aligned.[3]

B. Thermochemistry of the Iodohaloethanes

Measurements of the **minimum** recoil energy of the stable radical correspond by energy conservation to the **maximum** internal energy at which the CX_2CZ_2-Y radical survives before C-Y bond fission. The

difference between this threshold translational energy and the available energy is an upper limit to the sum of the C-I and C-Y bond strengths. This sum is the enthalpy of reaction ΔH_R at 0 K for Y-CX_2CZ_2-I → I + Y + CX_2CZ_2, and its value determines the heat of formation of the parent iodohaloethane, since the product thermochemistry is known. In this experiment, we measured the following bounds to the reaction enthalpies and heats of formation at 0 K:

(1) $CF_2ICF_2Br \rightarrow I + Br + CF_2CF_2$

$\Delta H_R \leq 73.8 \pm 2$ kcal/mol, $\Delta H^\circ_{f,0}(CF_2ICF_2Br) \geq -176.6 \pm 2.7$ kcal/mol 308 nm

$\Delta H_R \leq 74.8 \pm 1$ kcal/mol, $\Delta H^\circ_{f,0}(CF_2ICF_2Br) \geq -177.6 \pm 1.7$ kcal/mol 266 nm

(2) $CF_2ICF_2I \rightarrow I + I + CF_2CF_2$

$\Delta H_R \leq 59.1 \pm 1$ kcal/mol, $\Delta H^\circ_{f,0}(CF_2ICF_2I) \geq -164.4 \pm 1.7$ kcal/mol 308 nm

Errors are propagated assuming that the uncertainties are additive, since different literature values are used and the statistical significances are difficult to compare. The results for CF_2ICF_2Br at 266 nm are refined values of an earlier study by Krajnovich, Butler, and Lee,[3] and they supercede the values reported in Table VII of Ref. 2. Analogous values for CH_2ICH_2Br could not be determined since stable CH_2CH_2Br radicals were not observable at any of the three photodissociation wavelengths.

Our measurements of ΔH_R are upper bounds,[2] since greater internal energies will be required to surmount any potential or rotational barrier or to provide some minimum product excitation when the radical

decomposes. Thus, $Y\text{-}CX_2CZ_2$ falls apart only when its internal energy exceeds the sum of the C-Y bond strength **and** the barrier height, and by energy conservation the minimum translational energy E_{min} will be too low by the barrier energy. The measured $\triangle H_R = E_{avl} - E_{min}$ is then too high.

We originally hoped that analysis of the spontaneous dissociation of the radical would determine the barrier height, but at present the analysis is too uncertain. The fast peak in the $CF_2CF_2^*$ spectrum of CF_2ICF_2I at 308 nm in Fig. 8 indicates that the secondary products are recoiling at velocities corresponding to average translational energies of 3 to 5 kcal/mol for the primary I^* channel. A part of this fast recoil originates from rotation, resulting from the conversion of CF_2CF_2I rotational momentum J into orbital momentum L of the products, which separate with a finite tangential velocity. Assuming that CF_2ICF_2I dissociates as a rigid molecule with impact parameter b = 1.1 Å, then at the most probable translational energy E_T = 14 kcal/mol, $J = \mu v_{rel} b = 170\,\hbar$. If the CF_2CF_2-I bond stretches from 2.14 Å to ≈3 Å before dissociation,[23] then B ≈ .02 cm^{-1} for a C-C-I angle of 120°, and the c.m. secondary translational energy may approach 1.5 kcal/mol. This is energy originally in the radical as rotation that becomes product translation.

Potential energy barriers in halogen plus ethylene reactions are generally small, and accumulated evidence shows that Cl, F + CH_2=CH_2 proceed with activation energies E_{act} < 1 kcal/mol.[24] Benson and O'Neal estimate that E_{act} is less than 3 kcal/mol for Br + CH_2=CH_2.[5] E_{act} is believed to scale with the difference between the electron affinity

of the halogen atom and the ionization potential of the olefin,[24] so that E_{act} for Br + CF_2=CF_2 and CH_2=CH_2 should be similar. The activation energy for I + CF_2=CF_2 has to our knowledge not been measured. The secondary peak in the 308 nm $CF_2CF_2^*$ spectrum assigned to spontaneous dissociation suggests, however, that its value lies near 3 to 5 kcal/mol.

The reaction enthalpies determined here are then upper bounds to the sum of the two carbon - halogen bond energies in Y-CX_2CZ_2-I, Y = Cl, Br, I. Decomposing $\triangle H_R$ into individual C-I and C-Y bond strengths requires further assumptions. The difference between $\triangle H_R$ for CF_2ICF_2I and CF_2ICF_2Br, 15.2 ± 1.5 kcal/mol, is very close to the difference in CF_3CF_2-I and CF_3CF_2-Br bond energies, 15.8 ± 2 kcal/mol, measured by Wu and Rodgers.[25] The similarity between these values implies that the β-iodine atom affects the C-Br and C-I bonds nearly equally. Assuming that the C-I bond energies in the two iodohaloethane compounds are the same, and equal to $D_0^\circ(CF_3CF_2\text{-I})$ = 52 ± 1.3 kcal/mol, we can estimate upper limits to the radical bond energies, CF_2CF_2-I(Br) → CF_2=CF_2 + I(Br), of 7.1 ± 2.5 kcal/mol for C-I and 22.3 ± 2.5 kcal/mol for C-Br. These values will be reduced if $\triangle H_R$ is too large or if the primary C-I bond in the parent molecule is stronger than the C-I bond in the CF_3CF_2-I analogue. On experimental grounds, this C-I bond energy difference should not be more than 3 kcal/mol since the $P(E_T)$ curves for the I^* channels extend very close to the estimated available energies.[3,19] This uncertainty is substantial, however, for the weak bonds in haloethyl radicals.

The radical bond energies can be compared directly through

estimates of the π bond energy of $CF_2=CF_2$ using the operational definition[26]

$$E_\pi = D_0^\circ(CF_3CF_2\text{-}Y) - D_0^\circ(CF_2CF_2\text{-}Y)$$
$$= D_0^\circ(CF_3CF_2\text{-}Y) + D_0^\circ(YCF_2CF_2\text{-}I) - \Delta H_R$$
$$\approx D_0^\circ(CF_3CF_2\text{-}Y) + D_0^\circ(CF_3CF_2\text{-}I) - \Delta H_R.$$

This definition equates the π bond energy with the difference in C-Y bond energies in the parent and radical, since in the radical a π bond forms as the C-Y bond breaks. It thus assumes that the C-Y and π bond energies add independently in the radical and ignores interactions which may stabilize the radical and effectively strengthen the C-Y bond. The π bond energies determined by our experiments for CF_2CF_2Br and CF_2CF_2I are 45.3 ± 3.5 and 44.9 ± 3.5 kcal/mol, respectively.[27] They are very close, indicating that I and Br lead to similar stabilization, or that there is a fortuitous cancellation between the stabilization energy and the activation energy for C-Y bond fission. Since our ΔH_R values are upper bounds, the calculated E_π values are lower limits to the values defined by the above equation. Our estimated lower limit to the π bond energy of 45 kcal/mol is indeed lower than a previous measurement by 7 kcal/mol, determined by Wu, Pickard, and Rodgers[28] using Y equal to F in the definition above.

The origin of this discrepancy does not lie in the calculation of E_π. Rodgers and coworkers' value of the π bond energy is based on their earlier measurement of the heat of formation of CF_2ICF_2I of -157.1 ± 1, which is 7 ± 3 kcal/mol higher than our estimate from the value of ΔH_R.[30] Their value predicts that $D_0^\circ(CF_2CF_2\text{-}I)$ = -0.27 ± 3

kcal/mol, and thus that the radical may not be bound.[29] Similar calculations for $D_0^o(CF_2CF_2\text{-}Br)$ also yield a value 7 kcal/mole lower than our upper estimate. The TOF spectra in Fig. 6 show, however, that the CF_2CF_2I radical can readily be synthesized; the width of the stable radical $P(E_T)$ is in agreement with the predicted 7 kcal/mol stability, and indicates that the radical can be created with a broad range of internal energies. These radicals, however, may be bound by rotational and potential energy barriers that sum to 7 kcal/mol. The average recoil of CF_2CF_2 and I during spontaneous dissociation of 3 to 5 kcal/mol is in accord with such a barrier, but the analysis is complicated by substantial averaging during secondary dissociation and by the possible interference of photon-induced radical decomposition even at low laser fluences. The similar E_T estimate from the CF_2BrCF_2I experiments makes explanations that rely solely on barriers less plausible, since the barrier to dissociation for $CF_2CF_2\text{-}Br$ should be smaller than for $CF_2CF_2\text{-}I$.

Our results do not yet unambiguously determine the origin of the 7 ± 2.5 kcal/mol barrier to dissociation. It may arise from a mechanical barrier to dissociation beyond a nearly zero C-I bond energy in the radical, or it may reflect a true difference in thermodynamic stability between CF_2CF_2I and C_2F_4 + I. We plan to extend these measurements to a third analogue, CF_2ClCF_2I, since C-Cl bond fission in the radical should proceed with very little activation energy. Regardless of the source of stability, the cumulative experiments described here show that large fluxes of intact haloethyl radicals can be created by photodissociation. This method promises

to be an important source of reactive starting compounds for future molecular beam experiments.

ACKNOWLEDGEMENTS

We thank Dr. Andrzej Rajca and Profs. Andrew Streitweiser and Alan Rodgers for enlightening discussions and Xinsheng Zhao and Eric Hintsa for their help. G. M. N. thanks the Miller Institute of the University of California for financial support. This work was supported by the Director, Office of Energy Research, Office of Basic Energy Sciences, Chemical Sciences Division of the U.S. Department of Energy under Contract No. DE-AC03-76SF00098.

References

1. a) T. K. Minton, P. Felder, R. J. Brudzynski and Y. T. Lee, J. Chem. Phys. **81**, 1759 (1984); b) T. K. Minton, G. M. Nathanson and Y. T. Lee, Laser Chem **7**, 297 (1987).
2. T. K. Minton, G. M. Nathanson and Y. T. Lee, J. Chem. Phys. **86**, 1991 (1984).
3. D. J. Krajnovich, L. J. Butler, and Y. T. Lee, J. Chem. Phys. **81**, 3031 (1984).
4. E. A. Carter and W. A. Goddard III, J. Phys. Chem. **90**, 998 (1986); J. Chem. Phys. **88**, 3132 (1988).
5. S. W. Benson and E. A. O'Neal, Kinetics of Gas Phase Unimolecular Reactions, NSRDS-NBS 21, p.611 (1970).
6. C. Taatjes and S. R. Leone, private communication.
7. R. S. Mulliken, Phys. Rev. **47**, 413 (1935).
8. S. J. Riley and K. R. Wilson, Faraday Discuss. Chem. Soc. **53**, 132 (1972).
9. F. G. Godwin, C. Paterson, and P. A. Gorry, Mol. Phys. **61**, 827 (1987); C. Paterson, F. G. Godwin, and P. A. Gorry, ibid. **60**, 729 (1987).
10. L. J. Butler, Ph.D. thesis, University of California, Berkeley, CA (1985).
11. R. N. Zare, Mol. Photochem. **4**, 1 (1972).
12. P. M. Kroger and S. J. Riley, J. Chem. Phys. **70**, 3863 (1979). X. Zhao, W. B. Miller, E. H. Hintsa and Y. T. Lee, submitted to the Journal of Chemical Physics.
13. P. M. Kroger and S. J. Riley, J. Chem. Phys. **67**, 4483 (1977).
14. X. Zhao, G. M. Nathanson, and Y. T. Lee, to be published.

15. J. L. Knee, L. R. Khundkar, and A. H. Zewail, J. Chem. Phys. **83**, 1996 (1985).

16. J. M. Parson and Y. T. Lee, J. Chem. Phys. **56**, 4658 (1972).

17. E. A. Carter and W. A. Goddard III, J. Am. Chem. Soc. **110**, 4077 (1988) and references therein.

18. See also T. K. Minton, Ph.D. thesis, University of California, Berkeley, CA (1986).

19. Q. Zhu, J. R. Cao, Y. Wen, J. Zhang, X. Zhong, Y. Huang, W. Fang, and X. Wu, Chem. Phys. Lett **144**, 486 (1988).

20. F. G. Godwin, P. A. Gorry, P. M. Hughes, D. Raybone, T. M. Watkinson, and J. C. Whitehead, Chem. Phys. Letts. **135**, 163 (1987).

21. G. E. Busch and K. R. Wilson, J. Chem. Phys. **56**, 3626 (1972).

22. G. Serboli and B. Minasso, Spectrochimica Acta **27a**, 1175 (1971); K. Tanabe, ibid **28a**, 407 (1972); K. Takagi, P.-K. Choi and W. Seki, J. Chem. Phys. **79**, 964 (1983).

23. S. W. Benson, Acc. Chem. Res. **19**, 335 (1986); Thermochemical Kinetics, (John Wiley, New York, 1970).

24. G. N. Robinson, R. E. Continetti, and Y. T. Lee, J. Chem. Phys. **89**, 6226 (1988); J. M. Farrar and Y. T. Lee, J. Chem. Phys. **65**, 1414 (1976); J. A. Kerr and M. J. Parsonage, Evaluated Data on Gas Phase Addition Reactions, (CRC, Cleveland, 1972).

25. E-C. Wu and A. S. Rodgers, J. Am. Chem. Soc. **98**, 6112 (1976).

26. S. W. Benson, J. Chem. Ed. **42**, 502 (1965).

27. E_π was determined using $D_0^\circ(CF_3CF2\text{-}Br)$ = 67.6 ± 1.6 kcal/mol and $D_0^\circ(CF_3CF_2\text{-}I)$ = 52 ± 1.6 kcal/mol from ref.25, after

correcting for the thermal energy.

28. E-C. Wu, J. M. Pickard, and A. S. Rodgers, J. Phys. Chem. **79**, 1078 (1975).

29. Calculated from $\triangle H_f^\circ(298)$ = -159.1 ± 0.5 kcal/mol of ref. 28 by correcting for the thermal energy using vibrational frequencies from D. A. C. Compton and D. M. Rayner, J. Phys. Chem. **86**, 1628 (1982).

Table I

Experimental Conditions[a]

	CF_2ICF_2I	CF_2BrCF_2I		CH_2BrCH_2I	
Reservior temp (°C)	0	−13		40	
vapor pressure (torr)	6	12		4	
Nozzle temp (°C)	250 (50)	250		150	
wavelength (nm)	308	308	248	266	308
peak velocity (cm/s)	69300 (69100)	68100	63200	64800	63600
α[b] (cm/s)	5020 (4880)	5390	4550	5380	4580
Speed ratio, S[b]	13.8 (14.2)	12.6	13.9	14.8	13.9
laser energy (mJ/pulse)					
parallel	see text	9	7	19	14
perpendicular		14	12	17	21
spot size (cm^2)	0.01	0.01	0.02	0.06	0.01
total counts/pulse					
I^+ (20°)	0.6	0.5	1	0.8	1
$C_2X_4^+$ (20°)	0.15	0.2	-	0.08	-
Br^+ (20°)	-	0.1	0.3	0.6	0.06

[a] numbers refer to experiments with argon carrier gas; numbers in parantheses for CF_2ICF_2I refer to experiments using N_2 carrier gas

[b] incident molecule number density is $N(V) = v^2 \exp[-(\frac{v}{\alpha} - S)^2]$

Table II

Photodissociation Results

RYI	Wavelength (nm)	Iodine State	Fraction	E_{avl} (Kcal/mol)	$\langle E_T \rangle / E_{avl}$	Rigid Radical $\langle E_T \rangle / E_{avl}$	Soft Radical $\langle E_T \rangle / E_{avl}$	FWHM/$\langle E_T \rangle$	Anisotropy β	f_{rad}[a]
CF_2ICF_2I	308[b]	I	< .3	41	-	.86	.13	-	-	N
		I*	> .7	19	.7	.86	.13	.55	1.8	< .5
CF_2BrCF_2I	248[c]	I*	1.0	41	.48	.84	.15	.6	1.8	S
	266[c]	I*	1.0	34	.53	.84	.15	.6	1.8	.65
	308	I	.23	41	.60	.84	.15	.45	1.2-1.8	.65
		I*	.77	19	.73	.84	.15	.35	1.2-1.8	1.0
CF_2BrCH_2I	248	I	.25	59	.41	.62	.16	.3	1.6	S
		I*	.75	37	.41	.62	.16	.45	1.25	S
	266	I	.10	52	.45	.62	.16	.25	1.6	N
		I*	.90	30	.46	.62	.16	.35	1.6	S
	308	I	.67	37	.51	.62	.16	.3	1.2	S
		I*	.33	15	.65	.62	.16	.45	1.2	N
CH_2BrCH_2I	248[d]	I*	< 1	39	.48	.57	.19	.4	0.8-1.8	N
	266[b]	I	.1	53	.42	.57	.19	.25	-	N
		I*	.9	31	.47	.57	.19	.3	1.5-2.0	N
	308[e]	I	< 1	38	.43	.57	.19	.45	0.9-1.9	N

a) fraction of dissociation events that lead to observable stable radical: S = small amount observed, N = not observed.
b) I channel not clearly resolved.
c) Previously studied by Krajnovich, Butler, and Lee, ref. 3.
d) I channel may contribute up to 5%.
e) I* channel may contribute up to 20%.

Figure Captions

(1) UV absorption spectrum of CH_2BrCH_2I vapor. The central peak is assigned to the (I)5P → σ^* transition. The (Br)4P → σ^* transition occurs at shorter wavelengths, but is partly obscured by air absorption in the Cary 14 spectrometer.

(2) Laboratory TOF spectra of iodine atom recoil from CF_2BrCF_2I at 308 nm at three LAB angles. Circles are experimental points, and the solid and dashed lines are the calculated fits using the $P(E_T)$ in the bottom panel. The dashed curves are the estimated contributions from the $I(^2P_{3/2})$ and $I(^2P_{1/2})$ channels.

(3) TOF spectrum of $CF_2CF_2^+$ from CF_2BrCF_2I at 308 nm. The fast and slow peaks are dissociative ionization of stable CF_2CF_2Br from the I and I* channels. The dotted curve is the calculated spectrum assuming that all the I channel fragments were stable, and the shaded region highlights error limits to the trailing edge of the fast peak. The lower panel shows the $P(E_T)$ for the fast peak, which fixes E_{min} at 19 ± 2 kcal/mol.

(4) TOF spectrum of $CF_2CF_2^+$ from CF_2BrCF_2I at 266 nm. The shaded region is an estimate to the trailing edge of the spectrum normalized at zero signal level, calculated from the trial energy distributions shown in the lower panel. E_{min} = 11 ± 1 kcal/mol.

(5) Iodine atom TOF spectra from CF_2ICF_2I at 308 nm. The curve in the middle panel was generated from the translational energy distribution in the bottom panel.

(6) TOF spectra of $CF_2CF_2^+$ and I^+ from CF_2ICF_2I at 308 nm near the stable CF_2CF_2 peak. Zero signal level represents the estimated trailing edge of the radical peak. The shaded regions are fits to this edge using the trial energy distributions shown in Fig. 7. E_{min} = 12 ± 2 kcal/mol in each case.

(7) Top panel: TOF spectrum of $C_2F_4^+$ from CF_2ICF_2I in N_2 at 250°C. Bottom panel: translational

energy distributions for stable CF_2CF_2I obtained by fitting the spectra in the top panels of Fig. 6 and of this figure. The two curves are **not** normalized with respect to each other.

(8) $C_2F_4^+$ and CF_2^+ TOF spectra from CF_2ICF_2I at 308 nm obtained using low and high laser powers, and with different temperature nozzles. The top panel shows the enhanced secondary dissociation of CF_2CF_2I at high nozzle temperature. The lower panels reveal an extra fast peak in the CF_2^+ TOF spectra that indicates secondary photodissociation of the radical into $CF_2 + CF_2 + I$.

(9) TOF spectra of iodine atom recoil from CH_2BrCH_2I at 266 nm. The dashed curves are the estimated contributions from the $I(^2P_{3/2})$ and $I(^2P_{1/2})$ channels using the translational energy distributions of Fig. 12.

(10) TOF spectra of iodine atom recoil from CH_2BrCH_2I at 248 nm. Only the overall fit is shown, using the $P(E_T)$ in Fig. 12.

(11) TOF spectra of iodine atom recoil from CH_2ICH_2Br at 308 nm. Only one component is dominant, assigned to the $I(^2P_{3/2})$ channel using the $P(E_T)$ in Fig. 12. The $I(^2P_{1/2})$ channel may account for up to 20% of the signal.

(12) Center-of-mass translational energy distributions for primary C-I bond fission in CH_2BrCH_2I at 248, 266, and 308 nm.

(13) Bromine TOF spectra of CH_2BrCH_2I at 308 and 248 nm. The solid curves are the calculated Br^+ signal from dissociative ionization of CH_2CH_2Br recoiling from the I atom, assuming that no radicals decompose. The dashed curves in the 248 nm spectra are fits assuming primary C-Br bond fission.

(14) TOF spectra at m/e = 26 and 79 for CH_2BrCH_2I at 266 nm. The solid and dashed curves are the calculated fits from dissociative ionization of CH_2CH_2Br recoiling from the I atom in the $^2P_{3/2}$ and $^2P_{1/2}$ states. The poor agreement indicates that very little if any stable CH_2CH_2Br radical is produced.

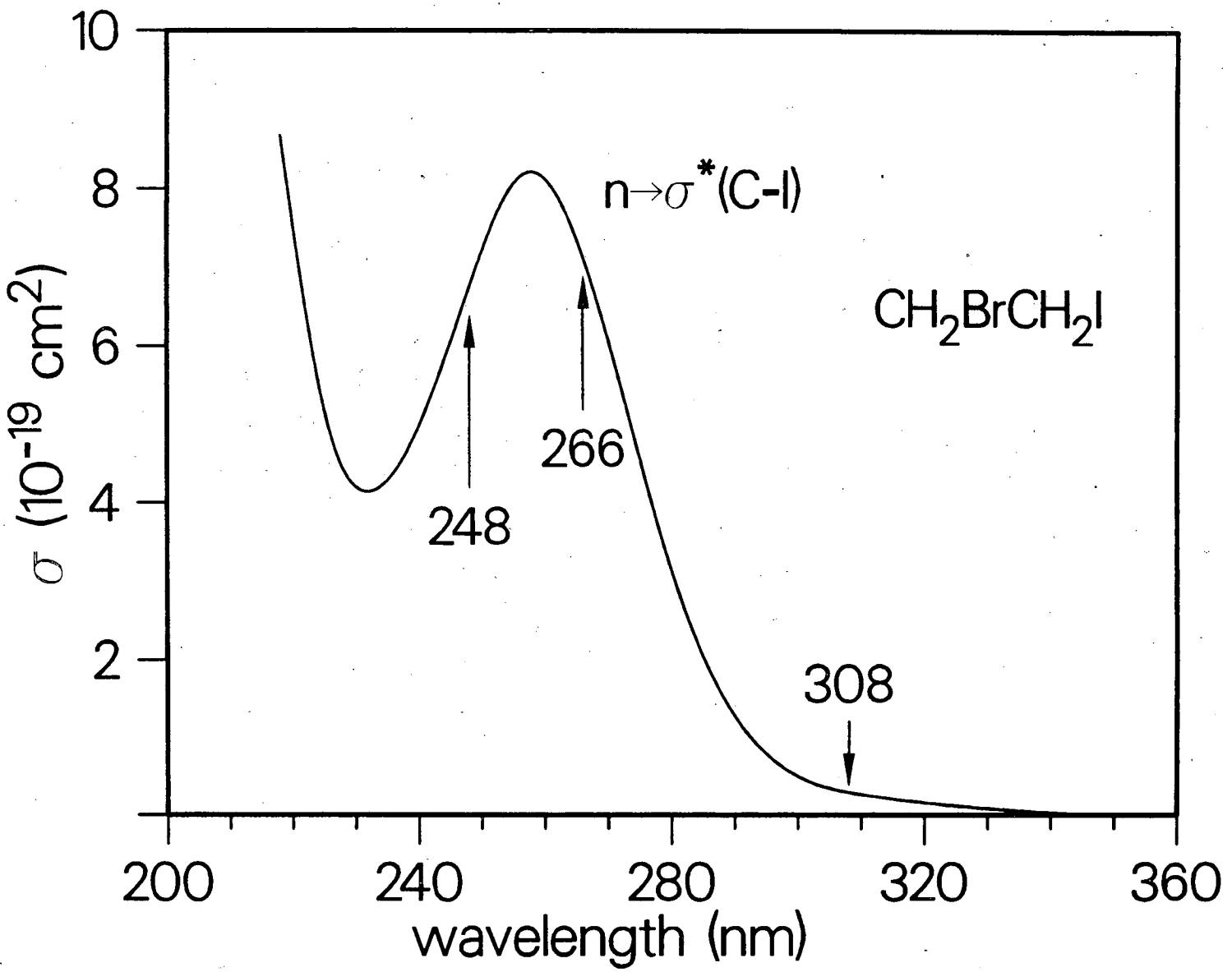

XBL 886-2173

Fig. 1

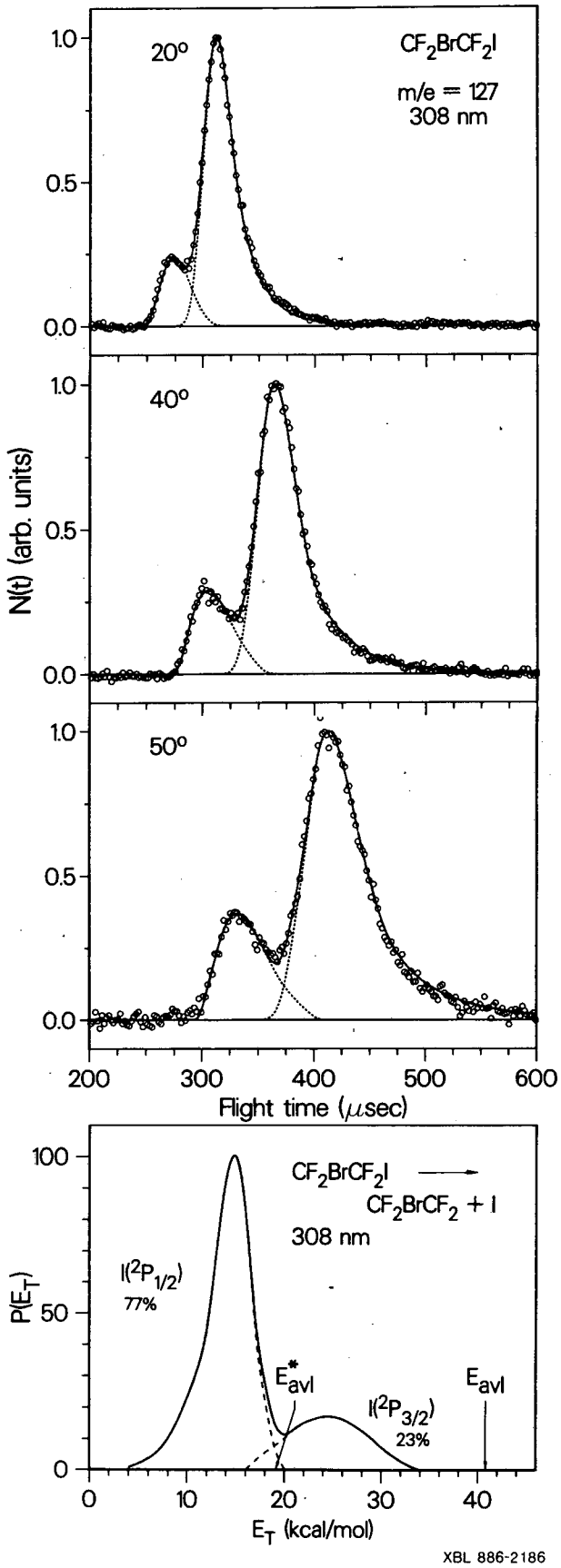
20°
40°
50°
CF_2BrCF_2I
m/e = 127
308 nm
N(t) (arb. units)
Flight time (μsec)
$CF_2BrCF_2I \longrightarrow CF_2BrCF_2 + I$
308 nm
$I(^2P_{1/2})$
77%
$I(^2P_{3/2})$
23%
E^*_{avl}
E_{avl}
$P(E_T)$
E_T (kcal/mol)
XBL 886-2186

Fig. 2

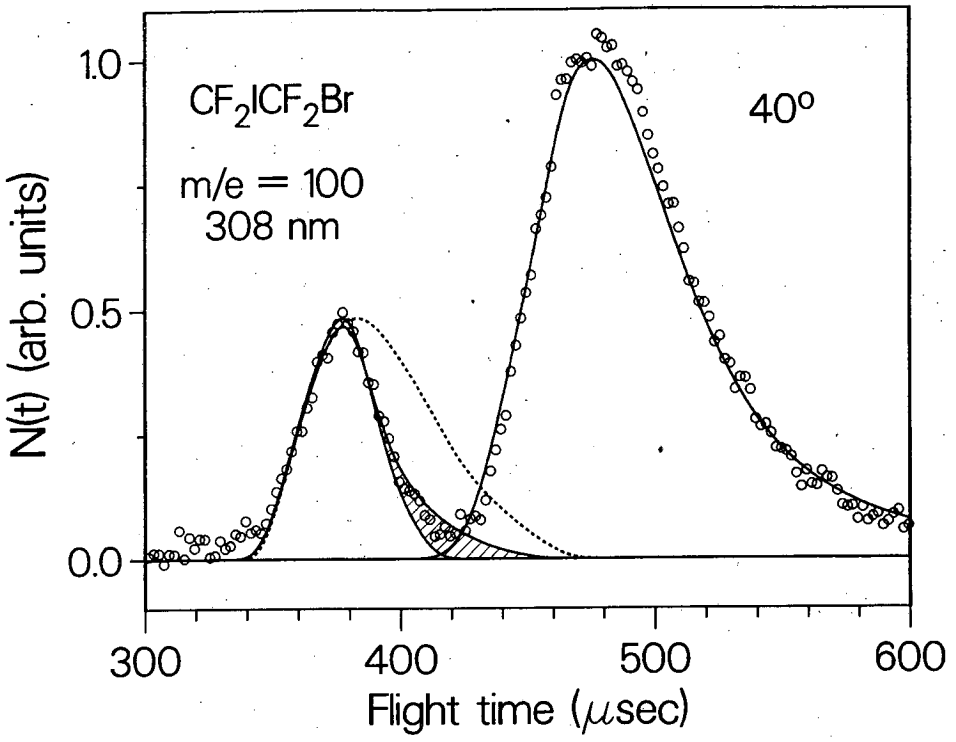

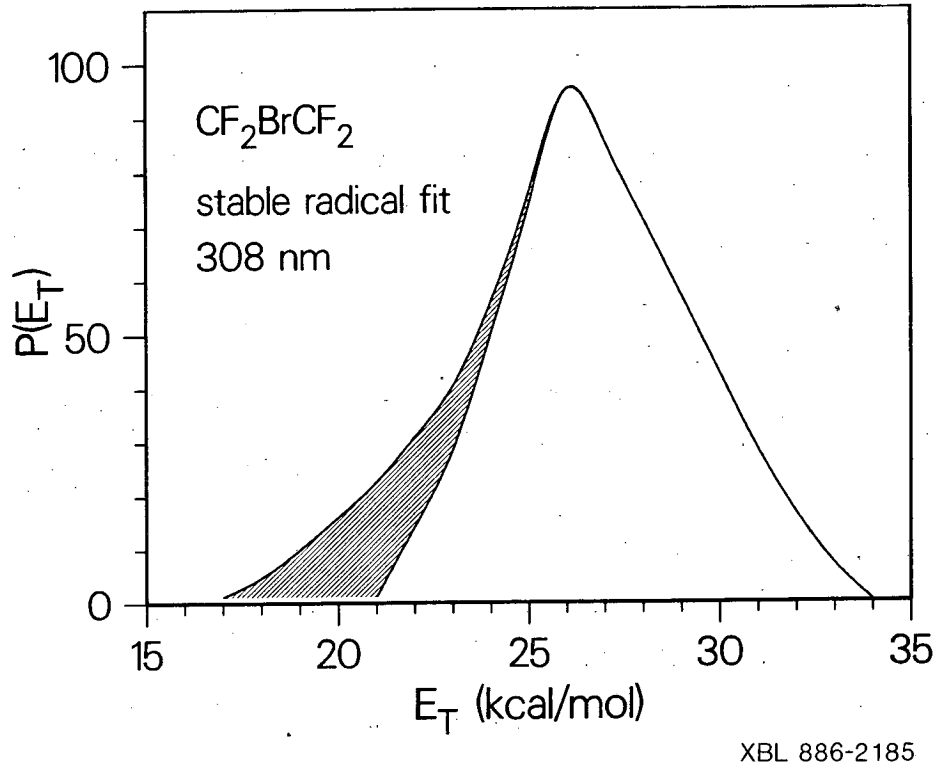

XBL 886-2185

Fig. 3

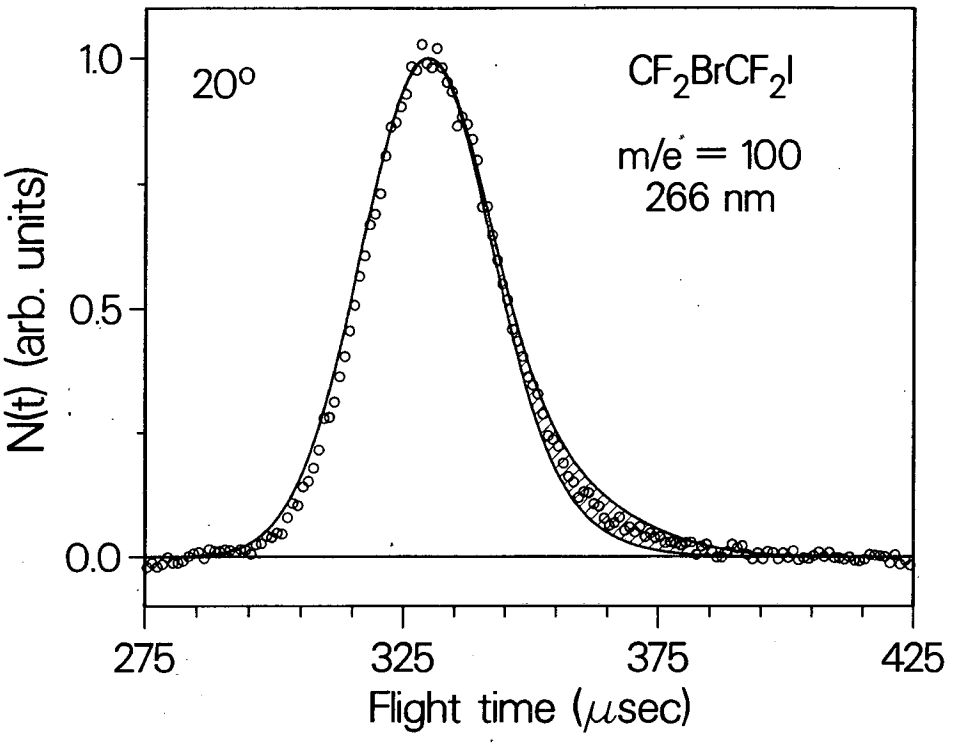

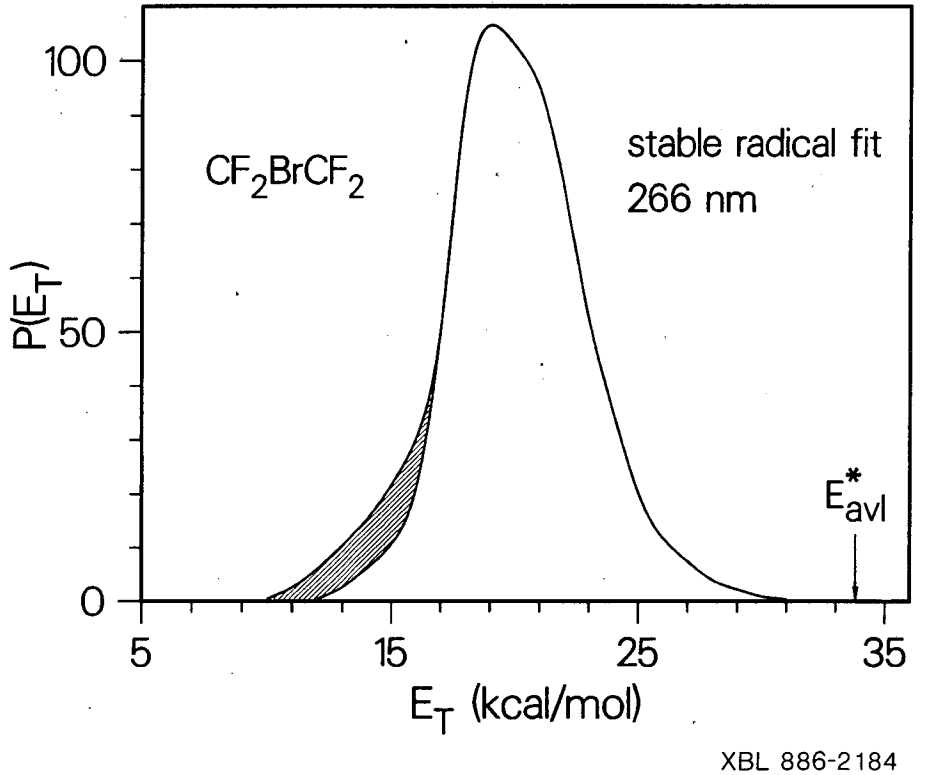

XBL 886-2184

Fig. 4

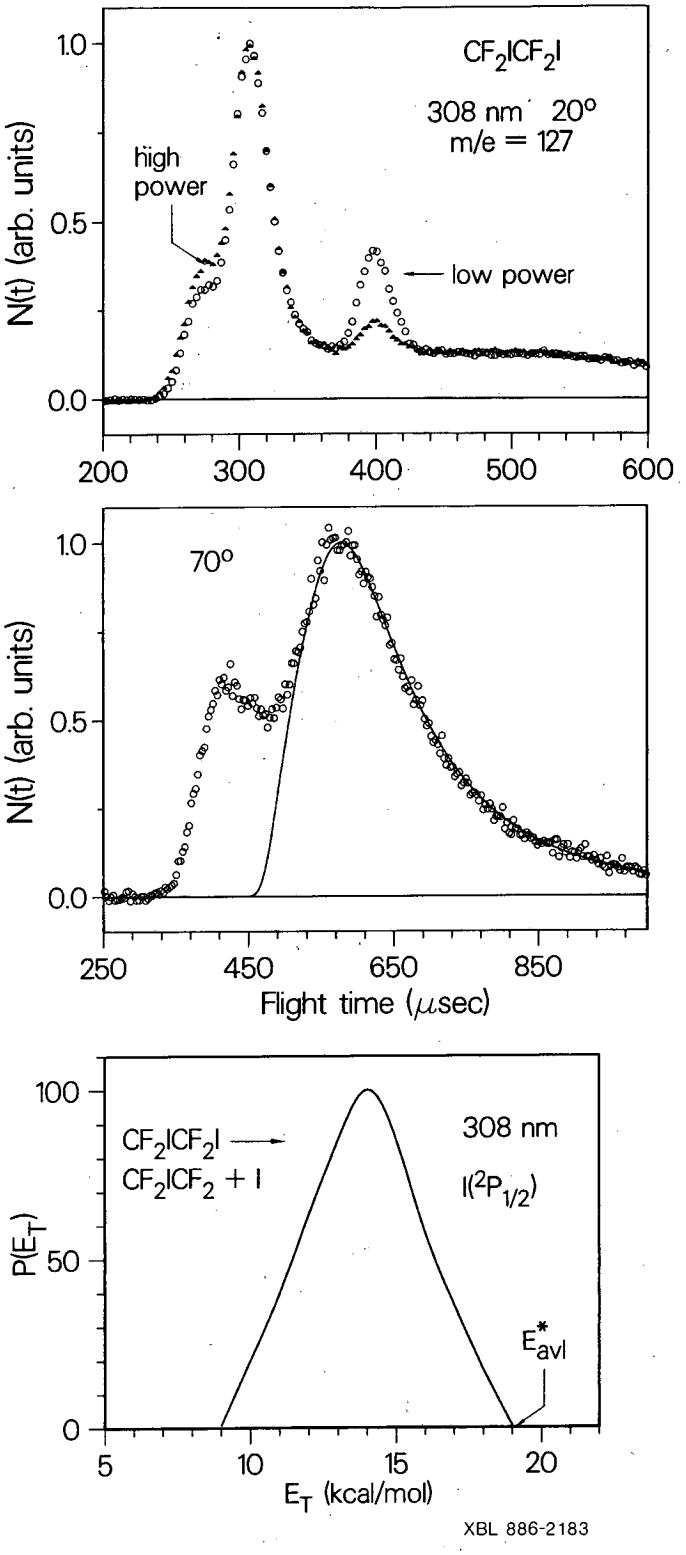
CF_2ICF_2I
308 nm 20°
m/e = 127
high power
low power
N(t) (arb. units)
1.0
0.5
0.0
200
300
400
500
600
70°
250
450
650
850
Flight time (μsec)
100
50
0
$P(E_T)$
$CF_2ICF_2I \rightarrow CF_2ICF_2 + I$
308 nm
$I(^2P_{1/2})$
E^*_{avl}
5
10
15
20
E_T (kcal/mol)
XBL 886-2183

Fig. 5

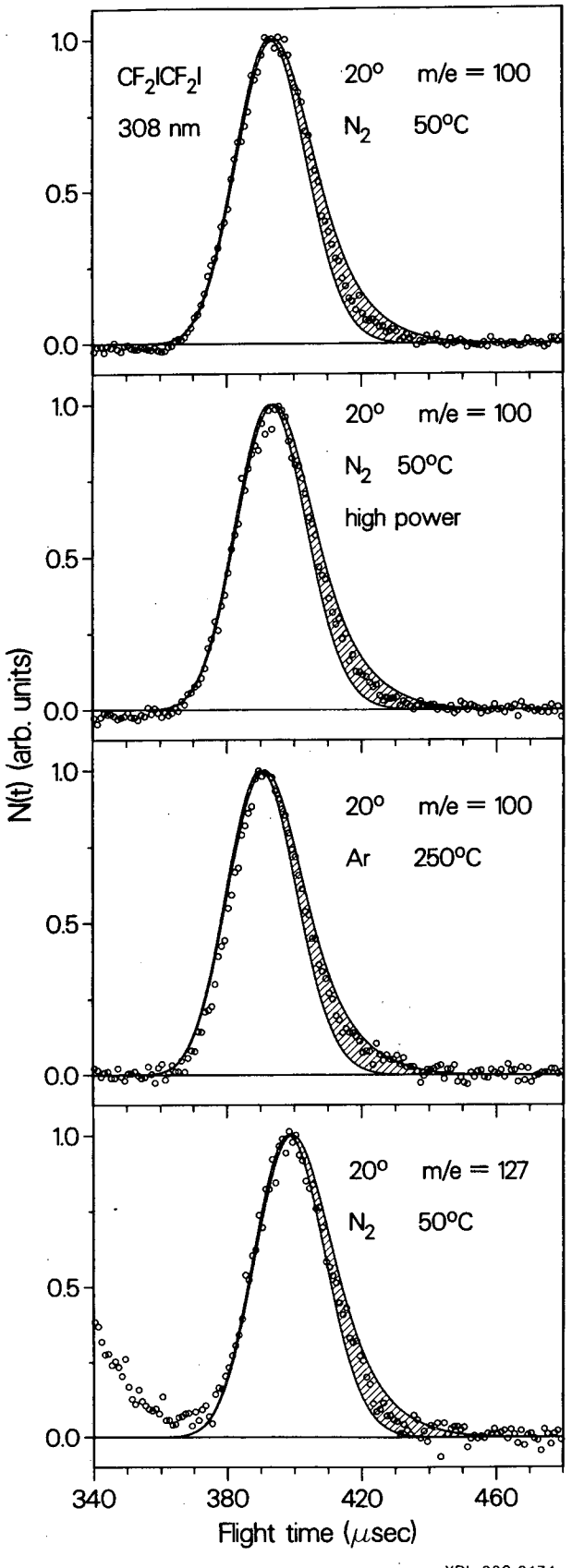

XBL 886-2174

Fig. 6

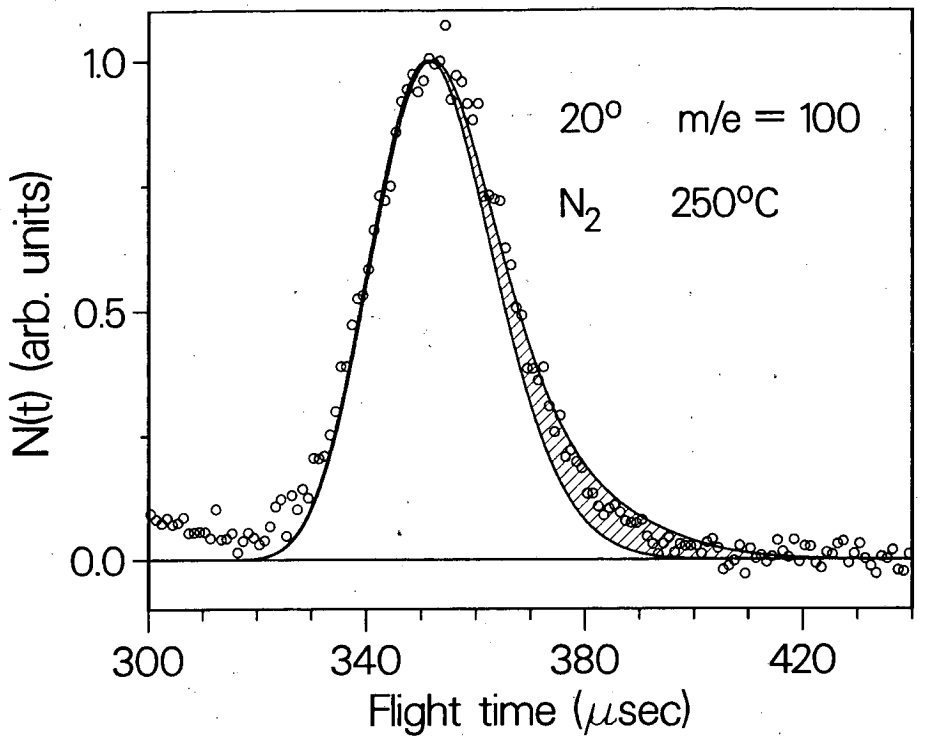

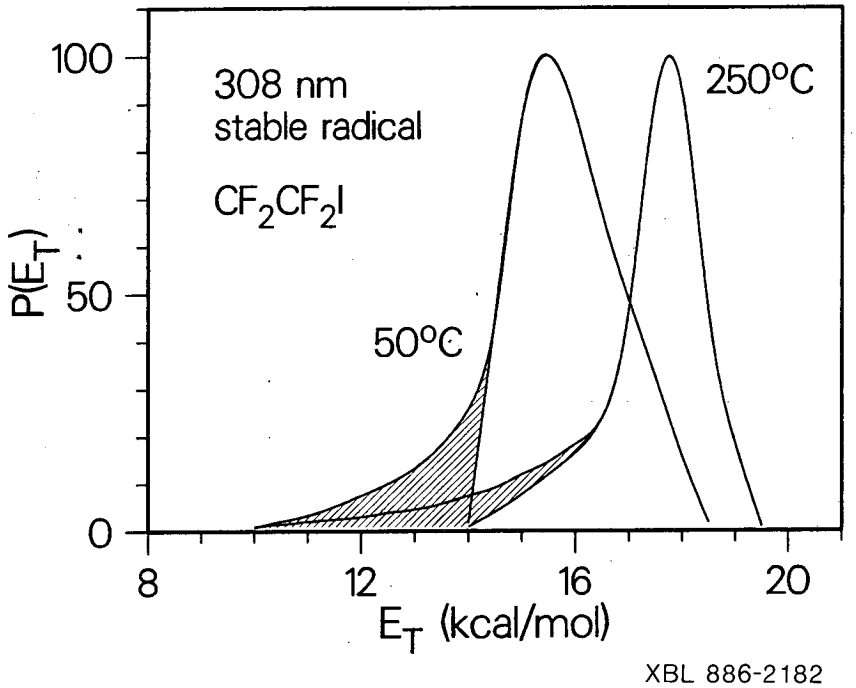

XBL 886-2182

Fig. 7

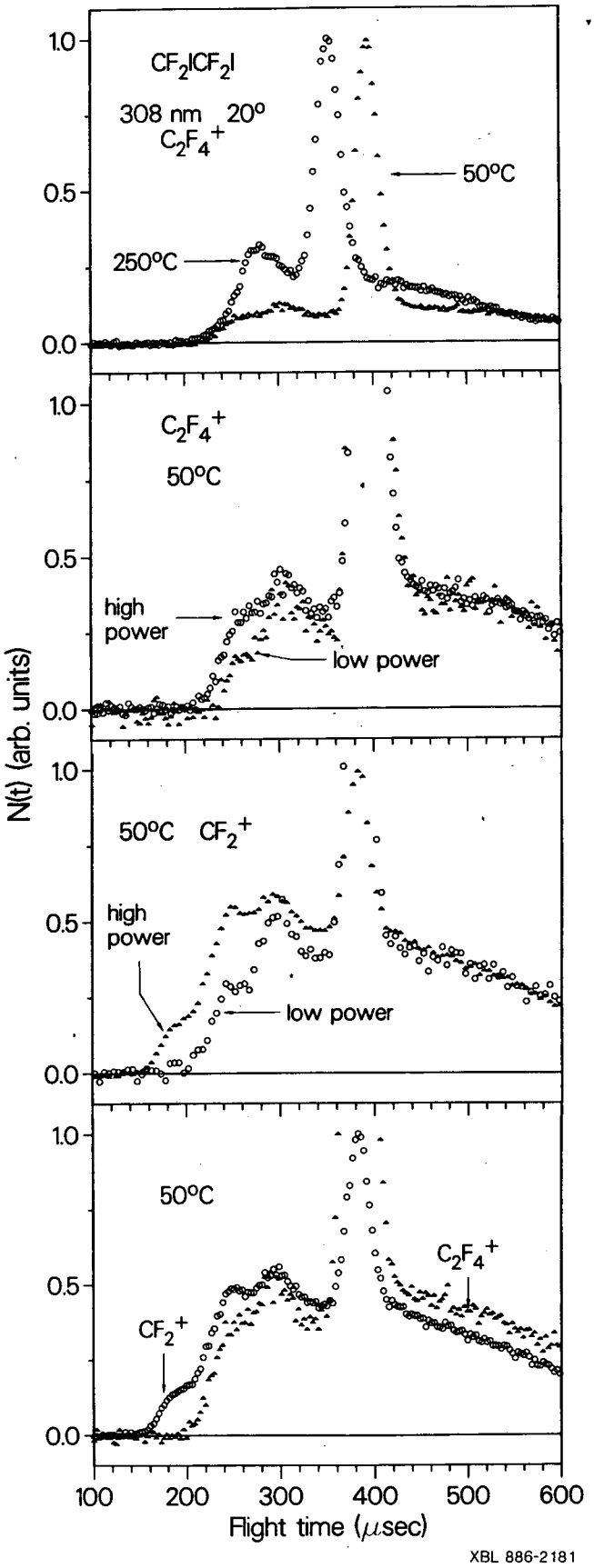
CF_2ICF_2I
308 nm 20°
$C_2F_4^+$
50°C
250°C
$C_2F_4^+$
50°C
high power
low power
50°C CF_2^+
high power
low power
50°C
$C_2F_4^+$
CF_2^+
N(t) (arb. units)
1.0
0.5
0.0
100
200
300
400
500
600
Flight time (μsec)
XBL 886-2181

Fig. 8

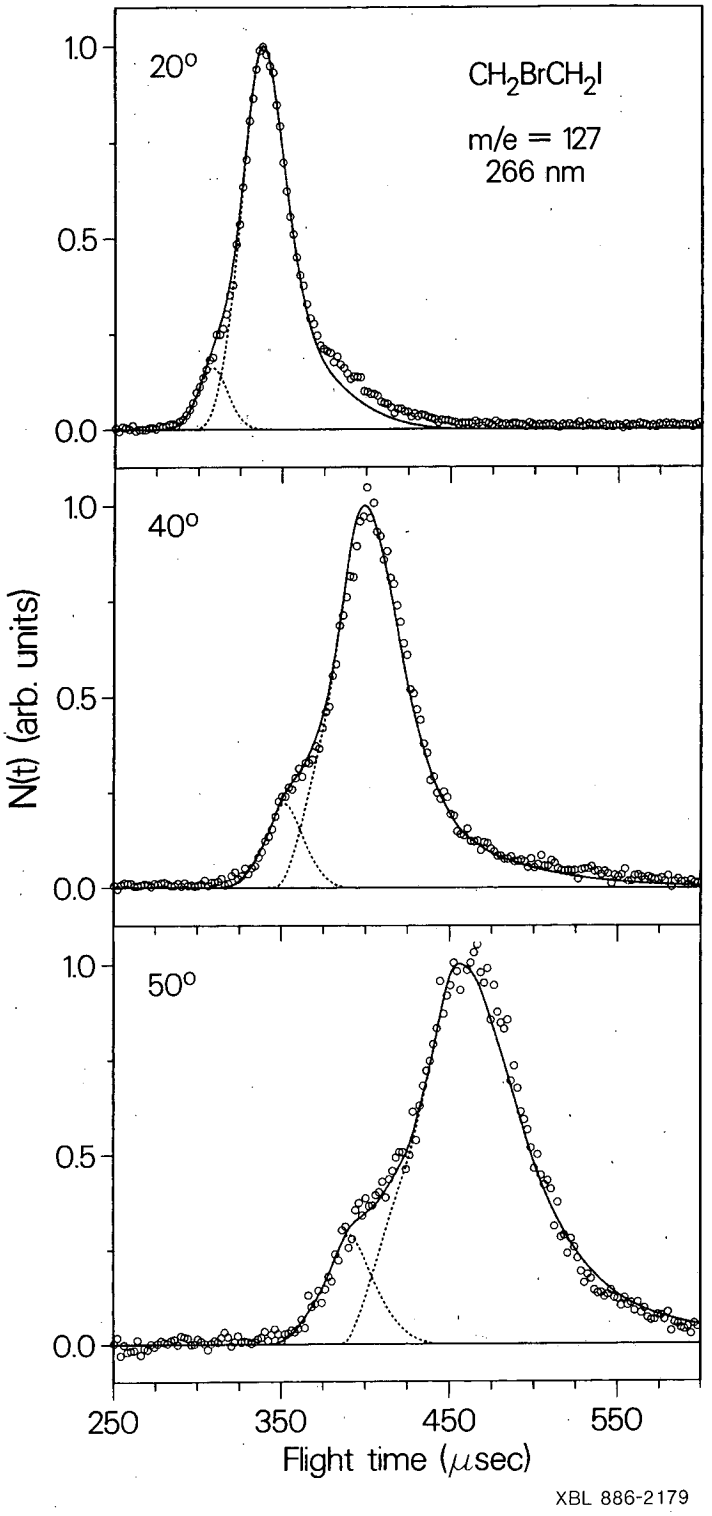
20°
40°
50°
CH_2BrCH_2I
m/e = 127
266 nm
1.0
0.5
0.0
N(t) (arb. units)
250
350
450
550
Flight time (μsec)
XBL 886-2179

Fig. 9

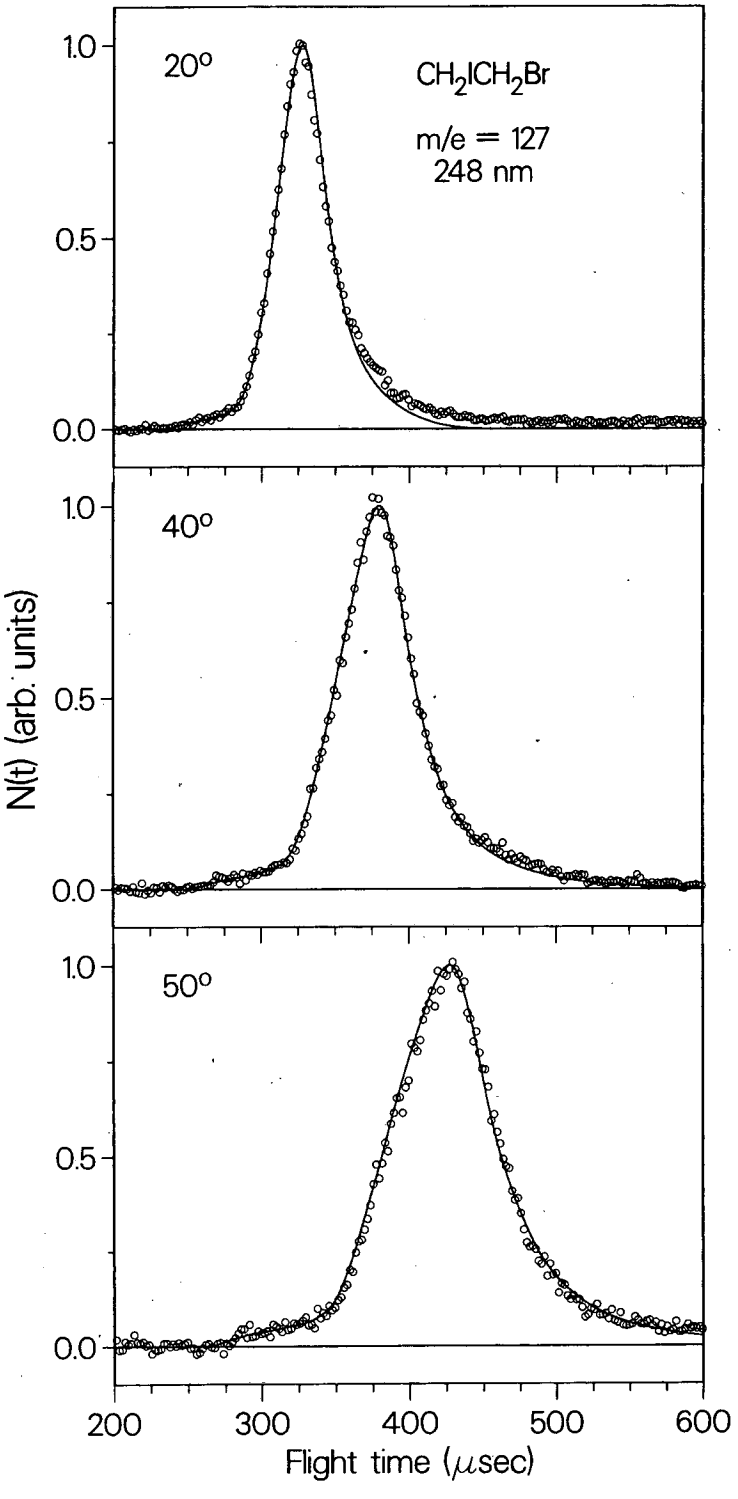

XBL 886-2178

Fig. 10

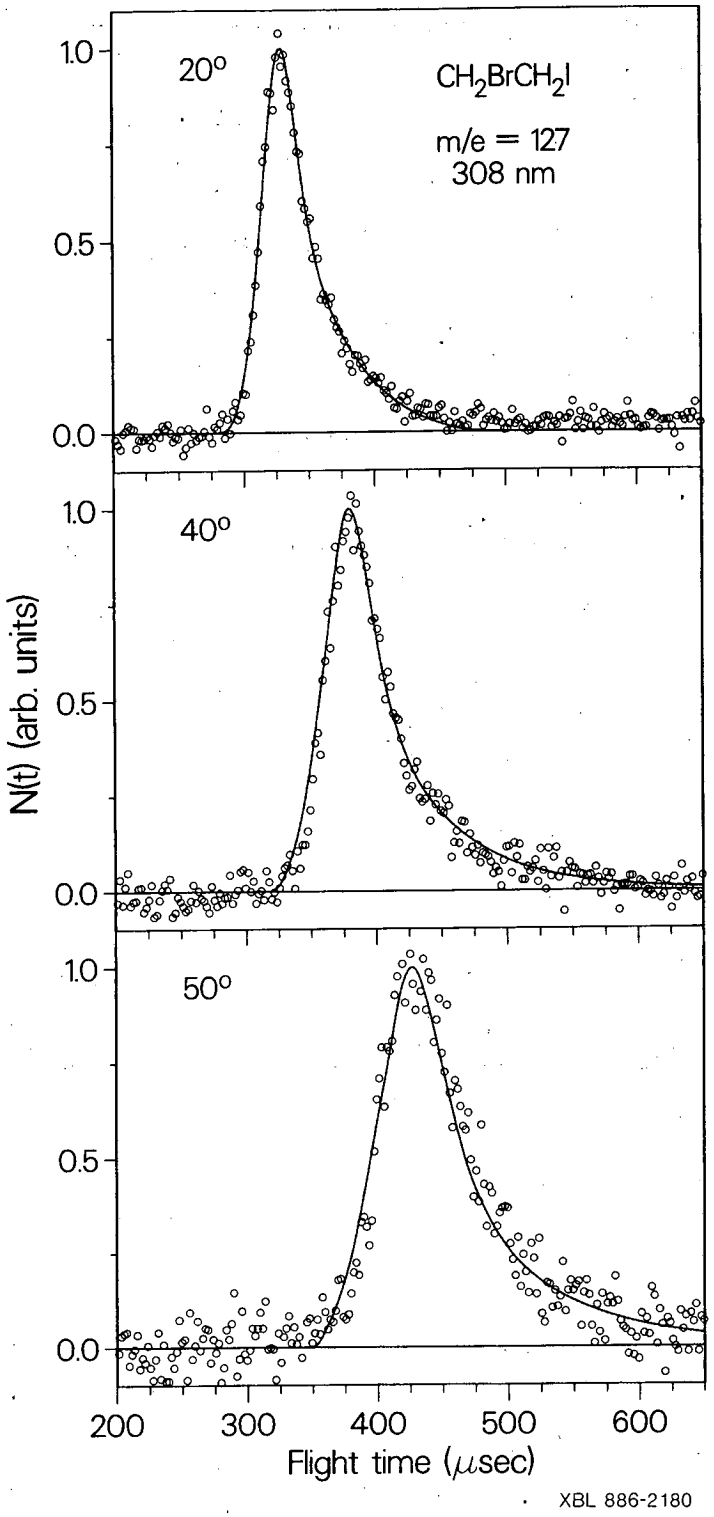
20°
40°
50°
CH_2BrCH_2I
m/e = 127
308 nm
1.0
0.5
0.0
N(t) (arb. units)
200
300
400
500
600
Flight time (μsec)
XBL 886-2180

Fig. 11

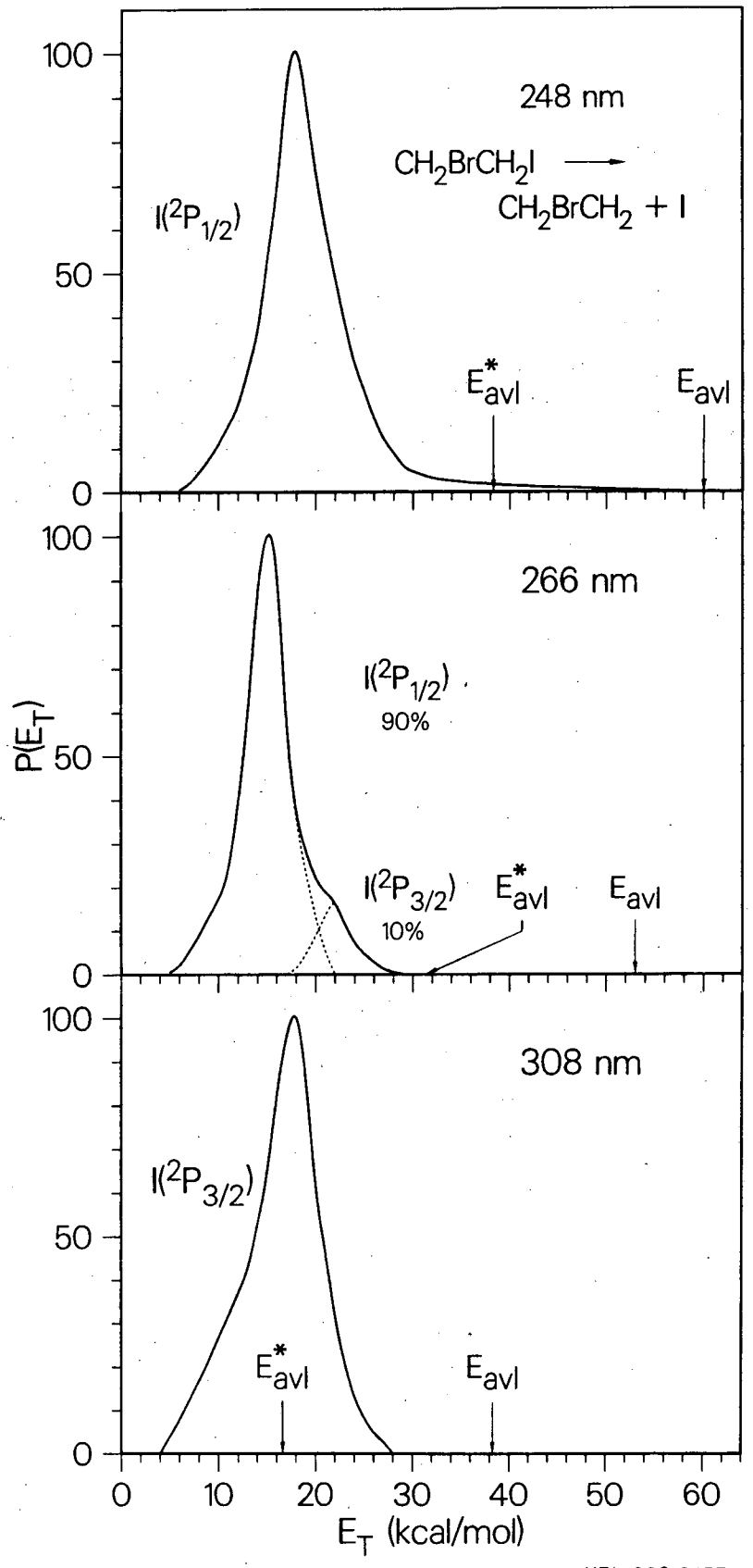

XBL 886-2177

Fig. 12

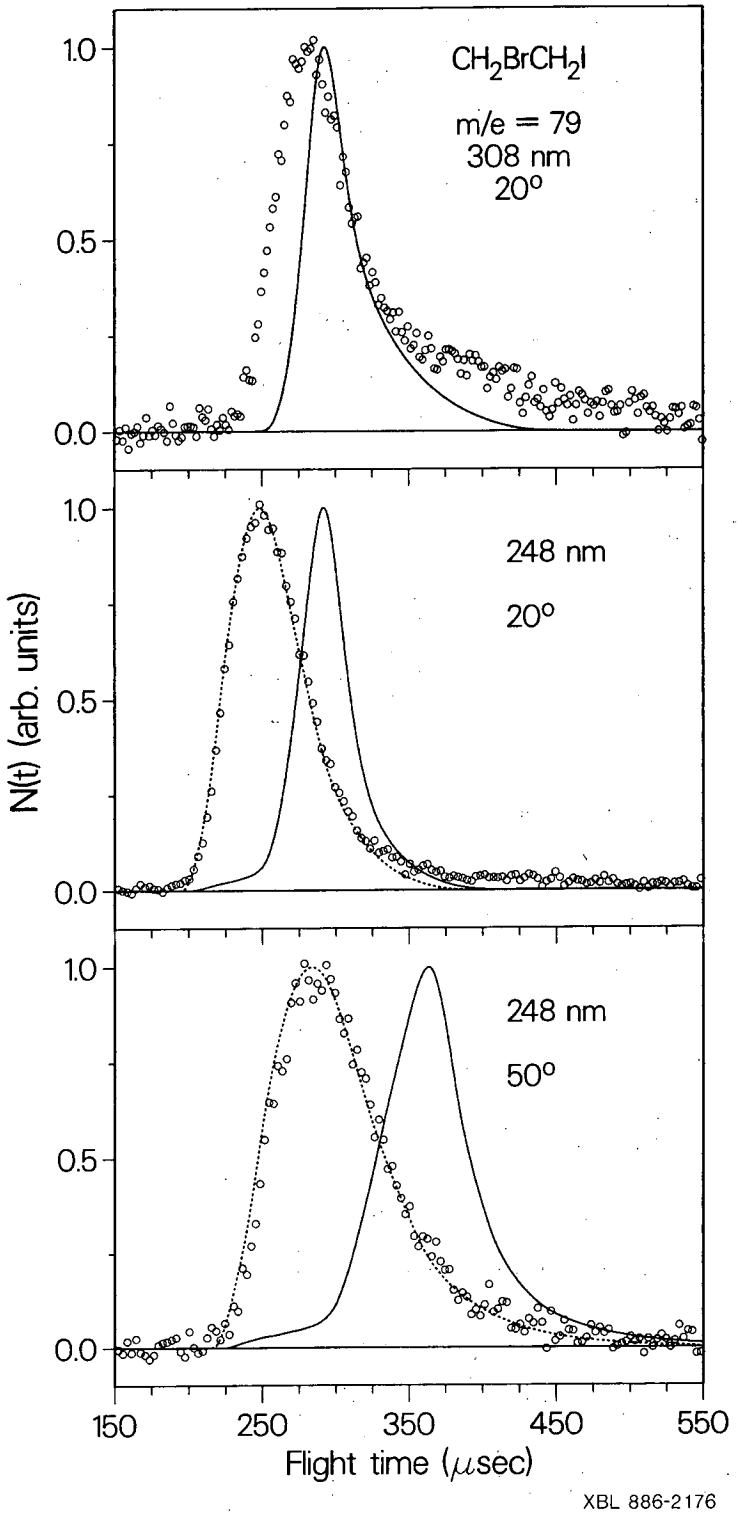
CH_2BrCH_2I
m/e = 79
308 nm
20°
248 nm
20°
248 nm
50°
N(t) (arb. units)
1.0
0.5
0.0
150
250
350
450
550
Flight time (μsec)
XBL 886-2176

Fig. 13

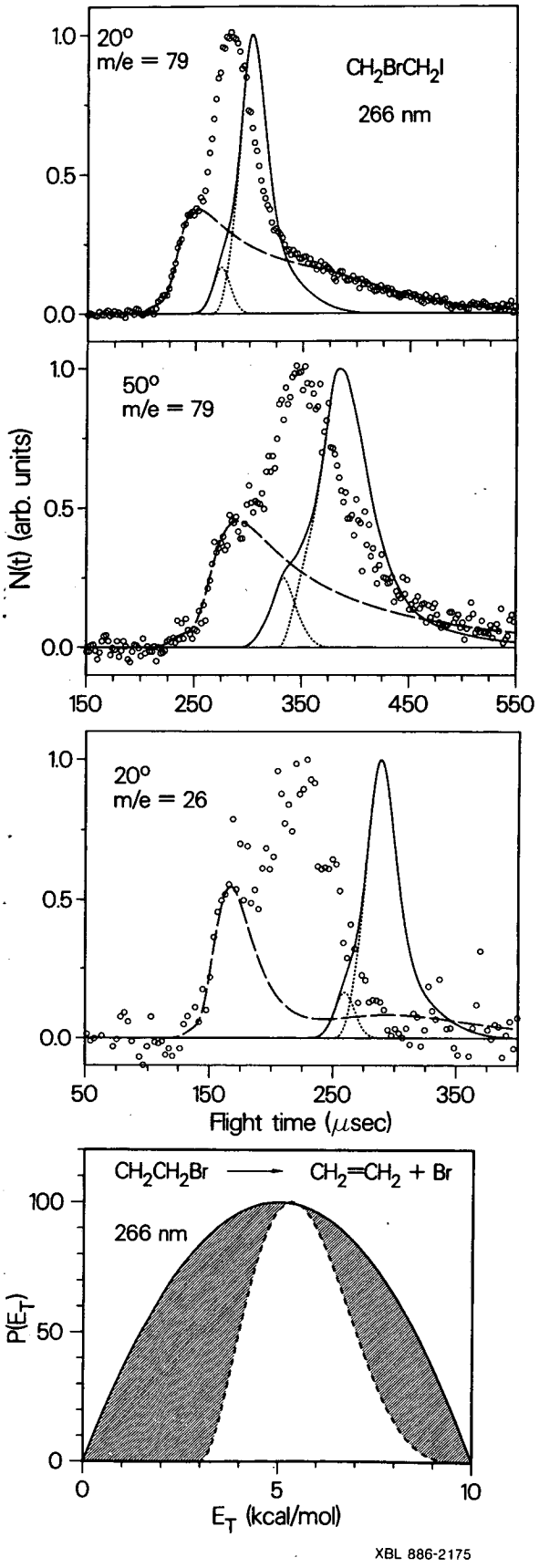
20°
m/e = 79
CH_2BrCH_2I
266 nm
50°
m/e = 79
N(t) (arb. units)
20°
m/e = 26
Flight time (μsec)
$CH_2CH_2Br \longrightarrow CH_2{=}CH_2 + Br$
266 nm
$P(E_T)$
E_T (kcal/mol)
XBL 886-2175

Fig. 14

LAWRENCE BERKELEY LABORATORY
TECHNICAL INFORMATION DEPARTMENT
1 CYCLOTRON ROAD
BERKELEY, CALIFORNIA 94720